Phylogenomics of a new fungal phylum reveals multiple waves of reductive evolution across Holomycota

Luis Javier Galindo[1], Purificación López-García[1], Guifré Torruella[1], Sergey Karpov[2] and David Moreira[1]

[1]Ecologie Systématique Evolution, CNRS, Université Paris-Saclay, AgroParisTech, Orsay, France.

[2]Department of Invertebrate Zoology, Faculty of Biology, St Petersburg State University, Russia

* Corresponding authors

E-mails: david.moreira@u-psud.fr; luisjagg92@gmail.com

Abstract

Compared to well-known multicellular fungi and unicellular yeast, unicellular fungi with zoosporic, free-living flagellated stages remain poorly known and their phylogenetic position is often unresolved. Recently, 18S+28S rRNA gene molecular phylogenetic analyses of two atypical parasitic fungi with amoeboid zoospores and record-long simplified kinetosomes, *Amoeboradix gromovi* and *Sanchytrium tribonematis*, showed that they formed a monophyletic group without affinity with any known fungal clade. To assess their phylogenetic position and unique trait evolution, we sequenced single-cell genomes for both species. Phylogenomic analyses using 264 protein markers and a comprehensive taxon sampling retrieved and almost fully-resolved fungal tree with these species forming a well-supported, fast-evolving clade sister to Blastocladiomycota. Chytridiomycota branched as sister to all other fungi, and the zoosporic fungus *Olpidium bornovanus* as sister to non-flagellated fungi. Comparative genomic analyses across Holomycota revealed an atypically reduced metabolic repertoire for sanchytrids given their placement in the tree. We infer four independent flagellum losses from the distribution of over 60 flagellum-specific proteins across Holomycota. The highly reduced sanchytrid flagellar machinery, notably their long kinetosome, might have been retained to support a putative light-sensing lipid organelle. Together with their phylogenetic position, these unique traits justify the erection of the novel phylum Sanchytriomycota. Our results also show that most of the hyphal morphogenesis gene repertoire of multicellular Fungi had already evolved in early holomycotan lineages.

Key words: Fungi, Holomycota, phylogenomics, Sanchytriomycota, flagella, hyphae

Multicellularity independently evolved in Fungi and Metazoa from unicellular ancestors along their respective eukaryotic branches, Holomycota and Holozoa, within Opisthokonta[1]. The ancestor of this major eukaryotic supergroup originated ~1-1,5 Ga ago[2–4] and likely possessed one posterior flagellum for propulsion in aquatic environments[1]. This character has been retained in many modern fungal lineages at least during some life cycle stages[5,6]. Along the holomycotan branch, the free-living, non-flagellated nucleariid amoebae were the first to diverge, followed by the flagellated, phagotrophic, endoparasitic Rozellida (Cryptomycota)[7–9] and Aphelida[10], and the highly reduced, non-flagellated Microsporidia[11,12]. Aphelids branch as sister lineage to *bona fide*, osmotrophic, Fungi[13]. Within fungi, except for the secondary flagellar loss in the chytrid *Hyaloraphydium curvatum* [14], all known early divergent taxa are zoosporic, having at least one flagellated stage.

Zoosporic fungi are widespread in all ecosystems, from soils to marine and freshwater systems , from tropical to Artic regions[15,16]. They are highly diverse saprotrophs and/or parasites, participating in nutrient recycling through the "mycoloop"[17–20]. Initially considered monophyletic, zoosporic fungi were recently classified into Blastocladiomycota and Chytridiomycota[21], in agreement with multigene molecular phylogenies[13,21,22]. These two lineages appear sister to the three main groups of non-flagellated fungi, Zoopagomycota, Mucoromycota and Dikarya, for which a single ancestral loss of the flagellum has been proposed[23]. Characterizing the yet poorly-known zoosporic fungi is important to understand the evolutionary changes (e.g. flagellum loss, hyphae development) that mediated land colonization and the adaptation of fungi to plant-dominated terrestrial ecosystems[24,25]. This requires a well-resolved phylogeny of fungi including all main zoosporic lineages. Unfortunately, previous phylogenomic analyses did not resolve which zoosporic group, either Blastocladiomycota or Chytridiomycota, is sister to non-flagellated fungi[21,26,27]. This lack of resolution may derive from the old age of these splits (~0,5-1 Ga)[3,28,29] and the existence of several radiations of fungal groups, notably during their co-colonization of land with plants[25,30], which would leave limited phylogenetic signal to resolve these deep nodes[22].

Because of this phylogenetic uncertainty, the number and timing of flagellum losses in fungi remain under debate, with estimates ranging between four and six for the whole Holomycota[31]. Improving taxon sampling with new, divergent zoosporic fungi can help resolving these deep nodes. One of such organisms is *Olpidium*, a morphologically reduced parasite of plant roots, nematodes and rotifers[32,33]. Although several few-genes phylogenies suggested a

relationship with Zoopagomycota[26,31,34], its phylogenetic position remains unclear. Another interesting lineage of uncertain position is the sanchytrids, a group of chytrid-like parasites of algae represented by the genera *Amoeboradix* and *Sanchytrium*, which exhibit a highly reduced flagellum with an extremely long kinetosome[35,36]. Determining the phylogenetic position of these two zoosporic lineages remains decisive to infer the history of flagellum losses and the transition to hyphal-based multicellularity. With these objectives, we generated the first genome sequences for the sanchytrids *Amoeboradix gromovi* and *Sanchytrium tribonematis* and analysed them together with available genomic and transcriptomic data for *Olpidium*, Chytridiomycota and Blastocladiomycota. We obtained an almost fully-resolved phylogeny showing sanchytrids as a new fast-evolving lineage sister to Blastocladiomycota, and *Olpidium* as an independent lineage sister to the non-flagellated fungi. Contrasting with previous weakly-supported analyses[13,22,37–39], we robustly placed the root of the fungal tree between chytrids and all other fungi. Our new phylogenomic framework of Fungi supports a conservative model of four flagellum losses in Holomycota and highlights the importance of early-diverging unicellular Holomycota in the evolution of hyphal-based multicellularity.

Results and discussion

The new zoosporic fungal phylum Sanchytriomycota

We isolated individual sporangia of *Amoeboradix gromovi* and *Sanchytrium tribonematis* by micromanipulation and sequenced their genomes after whole genome amplification. After thorough data curation (see Methods), we assembled two high-coverage genome sequences (123.9X and 45.9X, respectively) of 10.5 and 11.2 Mbp, encoding 7,220 and 9,638 proteins, respectively (Table 1). Comparison with a fungal dataset of 290 near-universal single-copy orthologs[40] indicated very high completeness for the two genomes (92.41% for *A. gromovi*; 91.72% for *S. tribonematis*). The two sanchytrid genomes yielded similar sequence statistics (Table 1) but showed important differences with genomes from other well-known zoosporic fungi. They are five times smaller than those of Blastocladiomycota (40-50 Mb) and average chytrids (~20 to 101 Mb), an observation extensive to the number of protein coding genes. Their genome GC content (~35%) was much lower than that of Blastocladiomycota and most chytrids (40-57%, though some chytrids, like *Anaeromyces robustus*, can have values down to 16.3%[41,42]). Low GC

content correlates with parasitic lifestyle in many eukaryotes[43]. In Holomycota, low GC genomes are observed in microsporidian parasites and Neocallimastigomycota, both anaerobic and exhibiting reduced mitochondrion-derived organelles[42,44], and in the aerobic parasite *Rozella allomycis*[9]. Although sanchytrids are aerobic parasites with similar life cycles to those of Blastocladiomycota and chytrids[35,36,45], their smaller genome size and GC content suggest that they are more derived parasites. This pattern is accompanied by a global acceleration of evolutionary rate (see below), a trend also observed, albeit at lower extent, in *R. allomycis*[9,46–48].

The mitochondrial genomes of *S. tribonematis* and *A. gromovi* showed similar trends. Gene order was highly variable (Supplementary Fig. 1), as commonly observed in Fungi[49], and their size (24,749 and 27,055 bp, respectively) and GC content (25.86% and 30.69%, respectively) were substantially smaller than those of most other Fungi. However, despite these signs of reductive evolution, most of the typical core mitochondrial genes were present, indicating that they have functional mitochondria endowed with complete electron transport chains.

To resolve the previously reported unstable phylogenetic position of sanchytrids based on rRNA genes[35], we carried out phylogenomic analyses on a manually curated dataset of 264 conserved proteins (91,768 amino acid positions)[13,50,51] using Bayesian inference (BI) and maximum likelihood (ML) with the CAT[52] and PMSF[53] models of sequence evolution, respectively. Both mixture models are robust against homoplasy and long-branch attraction (LBA) artefacts[22,52]. We selected 69 species (dataset GBE69), including a wide representation of holomycota plus two holozoans, two amoebae and one apusomonad as outgroup. In addition to the new sanchytrid data, we incorporated several key zoosporic fungi: the two Blastocladiomycota *Paraphysoderma sedebokense*[54–56] and *Coelomomyces lativittatus*[57], the enigmatic flagellated fungus *Olpidium bornovanus*[58], and the non-flagellated chytrid *Hyaloraphidium curvatum*, thought to have completely lost its flagellum[14]. BI and ML phylogenomic analyses yielded the same tree topology for major fungal groups with only minor changes in the position of terminal branches (Fig. 1a). We recovered maximum statistical support for both the monophyly of sanchytrids (*A. gromovi* + *S. tribonematis*) and their sister position to Blastocladiomycota. Thus, sanchytrids form a new deep-branching zoosporic fungal clade. Given their divergence and marked genomic differences with their closest relatives (Blastocladiomycota), we propose to create the new phylum Sanchytriomycota to accommodate these fungal species (see description below).

The new phylogeny of Fungi

In addition to the strongly supported Sanchytriomycota phyl. nov. and Blastocladiomycota relationship, and contrasting with its previous unstable position in few-genes phylogenies[26,34], we retrieved *O. bornovanus* as an independent lineage branching as sister to the major non-flagellated fungal clade. Chytrids appeared as sister group of all other fungi with full Bayesian posterior probability (PP=1) but moderate ML bootstrap support (BS=79%). Despite the use of a large dataset, some branches remained unresolved, in particular the position of Glomeromycota sister either to Mucoromycota or Dikarya (Fig. 1a).

As observed in rRNA gene-based phylogenies[35], sanchytrids exhibited a very long branch (Fig. 1a), suggesting a fast evolutionary rate. Long branches associated with fast evolving genomes, well-known in Microsporidia[46] and other Holomycota, can induce LBA artefacts in phylogenetic analyses[59–61]. To ascertain if LBA affected the position of the fast-evolving sanchytrids and other fungi in our tree, we carried out several tests. First, we introduced in our dataset additional long-branched taxa, metchnikovellids and core Microsporidia, for a total of 84 species and 83,321 conserved amino acid positions (dataset GBE84). Despite the inclusion of these LBA-prone fast-evolving taxa, we recovered the same topology as with the previous taxon sampling with just minor position changes for lineages within large clades (Supplementary Fig. 2). Again, the sister relationship of sanchytrids and Blastocladiomycota and the monophyly of *O. bornovanus* and non-zoosporic fungi were fully supported. Chytrids were sister to all other fungi with full Bayesian PP and slightly higher ML BS (82%).

Second, we tested the influence of fast-evolving sites by applying a slow-fast approach[62] and progressively removing the fastest-evolving sites (in 5% steps) of both the 69- and 84-species alignments. The monophyly of sanchytrids and Blastocladiomycota obtained maximum support (>99% bootstrap) in all steps until only 25/20% (GBE69/GBE84) of the sites remained, when the phylogenetic signal was too low to resolve any deep-level relationship (Fig. 1b). The monophyly of sanchytrids and Blastocladiomycota was as strongly supported as that of Dikarya. A root of the fungal tree between sanchytrids + Blastocladiomycota and the rest of fungi always received poor support (<50% bootstrap). On the contrary, the root between chytrids and the rest of fungi was strongly supported (>90% bootstrap) by all datasets with 10% to 50% (GBE69) and 10% to 45% (GBE84) of the fast-evolving sites removed. The position of *Olpidium* as sister of the non-flagellated fungi also received high support (>95% bootstrap) until 25/60% (GBE69/GBE84) of

the fast-evolving sites were removed. Its previously proposed relationship with Zoopagomycota[21,26] was always poorly supported.

Third, we applied sequence recoding[63] to alleviate possible compositional biases in our data and, again, recovered the same tree topology for both BI and ML analyses except for minor changes in apical branches (Supplementary Fig. 3a-d). The general congruence between the recoded and non-recoded analyses indicates that our results were not disturbed by compositional biases.

Finally, we further tested the robustness of the position of chytrids and *Olpidium* using alternative topology (AU) tests. They did not reject alternative positions for the divergence of Chytridiomycota and Blastocladiomycota + Sanchytriomycota (*p*-values >0.05; Supplementary Table 2), which likely reflected the weak phylogenetic signal concerning these deep branches[22]. However, we observed that, for the two datasets of 69 and 84 species, the *p*-values of trees showing chytrids as sister group of all other fungi were higher than those of trees with Blastocladiomycota + Sanchytriomycota as the first fungal branch to diverge (Supplementary Table 2). In the case of *Olpidium*, all tests significantly rejected its relationship with Zoopagomycota, in particular a close association with Basidiobolaceae[26,31,34] (*p*-value <0.001), and supported its position as a new lineage sister to the large non-flagellated fungal clade (*p*-values 0.539 and 0.554 for GBE69 and GBE84, respectively). Based on the zoospore ultrastructure, *Olpidium* was also suggested to be related with *Caulochytrium protostelioides*[21,64]. However, *C. protostelioides* branched in our multi-gene phylogenies within Chytridiomycota with maximum support, confirming that ultrastructural similarity most likely reflects convergent evolution. All our results concur to confirm that *Olpidium* constitutes a new phylum-level fungal linage (Olpidiomycota) sister to the non-flagellated fungi, in agreement with recent unpublished work by Chang et al.[65].

The relative position of Chytridiomycota or Blastocladiomycota as first branch to diverge within Fungi has remained a major unresolved question[66]. If the earliest fungal split occurred ~1 billion years ago[29], the phylogenetic signal to infer it may have been largely eroded over time. Likewise, if radiation characterized early fungal evolution[22], the accumulation of enough sequence substitutions during diversification would have been limited. This would explain the difficulty to resolve the deepest branches of the fungal tree, the fact that Chytridiomycota and Blastocladiomycota have alternatively been recovered as sisters of all other fungi[21,26,27,39,65] and the low support and discrepancies observed for the split between Glomeromycota and

Mucoromycota (with additional constraints related to their symbiotic adaptation to land plants[24,67,68]). The solid position of the root of the fungal tree on the chytrid branch revealed by our phylogenomic analyses with a richer dataset is additionally consistent with the distribution of so-considered derived characters in Blastocladiomycota, including sporic meiosis, relatively small numbers of carbohydrate metabolism genes and, in some species, hyphal-like apical growing structures (*Allomyces*) and narrow sporangia exit tubes (e.g. *Catenaria* spp.)[5,69–71].

Macroevolutionary trends in primary metabolism

To assess if sanchytrid metabolic capabilities are as reduced as suggested by their small genome sizes, we inferred their metabolic potential in comparison with other major fungal clades as well as other opisthokonts and amoebozoa as outgroup (43 species). Only half of the predicted sanchytrid proteins could be functionally annotated using EggNOG[72] (3,838 for *A. gromovi*; 4,772 for *S. tribonematis*), probably due to the fact that, being fast-evolving parasites[35,36,45], many genes have evolved beyond recognition by annotation programs[73,74]. However, low annotation proportions are common in holomycotans, including fast-evolving parasites (e.g. only 20% and 52% of the genes of the Microsporidia *Nosema parisii* and *Encephalitozoon cuniculi* could be assigned to Pfam domains and GO terms[73,75]) but also the less fast-evolving metchnikovellids (*Amphiamblys* sp., 45.6%), rozellids (*R. allomycis*, 64.9%; *P. saccamoebae*, 66.7%) and Blastocladiomycota (*P. sedebokerense*, 66.8%; *Catenaria anguillulae*, 47.5%; *Blastocladiella britannica*, 44.1%). We then compared the annotated metabolic repertoires of holomycotan phyla by focusing on 1,158 orthologous groups distributed in eight primary metabolism categories. Unexpectedly, cluster analyses based on the presence/absence of these genes did not group sanchytrids with canonical fungi and their closest aphelid relatives (i.e. *Paraphelidium*), but with non-fungal parasites (*R. allomycis Mitosporidium daphniae* and *P. saccamoebae*) which show evidence of reductive genome evolution[9,11,76] (Fig. 2a). An even further metabolic reduction was observed in Neocallimastigomycota, gut-inhabiting symbiotic anaerobic chytrids[33,77,78]. A principal coordinate analysis of the same gene matrix confirmed this result (Fig. 2b).

At a more detailed level, the main differences in the metabolic complement of sanchytrids and that of canonical fungi (+*Paraphelidium*) concerned the carbohydrate and lipid transport and metabolism categories, for which sanchytrids clustered with rozellids (Supplementary Fig. 4). We further pairwise-compared KEGG[79] orthologs of sanchytrids against *R. allomycis* and the

blastocladiomycete *A. macrogynus* (as representative of the sanchytrid closest canonical fungal relatives). The comparative metabolic maps of *A. gromovi* and *S. tribonematis* contained 1,222 and 1,418 orthologous groups, respectively, whereas those of *R. allomycis* and *A. macrogynus* contained 845 and 4,860, respectively (Supplementary Fig. 5a-c). Blastocladiomycota and sanchytrids shared more similarities, including the maintenance of amino acid and nucleotide metabolism and energy production with a complete electron transport chain, which were largely lacking in *Rozella*[9,13]. Nonetheless, some reductive trend in energy production pathways could be observed in sanchytrid mitochondria, including the loss of ATP8, one F-type ATP synthase subunit, which is also absent or highly modified in several metazoans, including chaetognaths, rotifers, most bivalve molluscs, and flatworms[80,81]. *S. tribonematis* also lacked the NADH dehydrogenase subunit NAD4L (Supplementary Fig. 1), although this loss is unlikely to impact its capacity to produce ATP since *R. allomycis*, which lacks not only ATP8 but also the complete NADH dehydrogenase complex, still seems to be able to synthesize ATP[9].

Most carbohydrate-related metabolic pathways were retained in sanchytrids and canonical fungi except for the galactose and inositol phosphate pathways, absent in both sanchytrids and *Rozella*. Nonetheless, sanchytrids displayed a rich repertoire of carbohydrate-degrading enzymes (Supplementary Figs. 6-10), most of them being likely involved in the degradation of algal cell walls required for their penetration into the host cells[13,82,83]. However, the most important difference between sanchytrids and canonical fungi concerned lipid metabolism, with the steroids and fatty acids metabolism missing in sanchytrids and also in *Rozella*[9] (Supplementary Fig. 5d-i). Collectively, our data suggest that, compared to Blastocladiomycota and other fungal relatives, sanchytrids have undergone a metabolic reduction that seems convergent with that observed in the phylogenetically distinct rozellid parasites.

Convergent reductive flagellum evolution in Holomycota

The loss of the ancestral opisthokont single posterior flagellum in Fungi[84,85] is thought to have facilitated their adaptation to land environments[86]. The number and timing of flagellum losses along the holomycotan branch remains to be solidly established. The flagellum is completely absent in nucleariids[12,51] but is found in representatives of all other major holomycotan clades, including rozellids[87], aphelids[10], and various canonical fungal groups, namely chytrids[78], Blastocladiomycota[88], *Olpidium*[21,26], and sanchytrids[35,36,45], although the latter are atypical.

Sanchytrid amoeboid zoospores have never been observed swimming, but glide on solid surfaces via two types of pseudopods: thin filopodia growing in all directions and a broad hyaline pseudopodium at the anterior end. The posterior flagellum, rather described as a pseudocilium, drags behind the cell without being involved in active locomotion[35,36]. Its basal body (kinetosome) and axoneme ultrastructure differ from that of most flagellated eukaryotes. Instead of the canonical kinetosome with 9 microtubule triplets and axonemes with 9 peripheral doublets + 2 central microtubules[89], sanchytrids exhibit reduced kinetosomes (9 singlets in *S. tribonematis*; 9 singlets or doublets in *A. gromovi*) and axonemes (without the central doublet and only 4 microtubular singlets)[35,36]. Despite this substantial structural simplification, sanchytrid kinetosomes are among the longest known in eukaryotes, up to 2.2 µm[35,36]. Such long but extremely simplified kinetosomes have not been reported in any other zoosporic fungi, including Blastocladiomycota[90]. Some of them, including *P. sedebokerense* [91], branching early in our multi-gene phylogeny (Fig. 1a), display amoeboid zoospores during the vegetative cycle, flagellated cells being most likely gametes[90,92,93].

To better understand flagellar reduction and loss across Holomycota, we analysed 61 flagellum-specific proteins on a well-distributed representation of 48 flagellated and non-flagellated species. Sanchytrids lacked several functional and maintenance flagellar components (Fig. 3a), namely axonemal dyneins, single-headed and double-headed inner arm dyneins, all intraflagellar transport proteins (IFT) of the group IFT-A and several of the group IFT-B. Sanchytrid kinetosomes also lost several components of the centriolar structure and tubulins, including Centrin2, involved in basal body anchoring[94], and Delta and Epsilon tubulins, essential for centriolar microtubule assembly and anchoring[95]. These losses (Fig. 3b) explain why sanchytrids lack motile flagella. Cluster analyses based on the presence/absence of flagellar components (Supplementary Fig. 11) showed sanchytrids at an intermediate position between flagellated and non-flagellated lineages. Therefore, sanchytrids are engaged in an unfinished process of flagellum loss, thereby providing an interesting model to study intermediate steps of this reductive process.

In addition to sanchytrid reduction, between four and six independent flagellar losses have been inferred in Holomycota[31]. Our new, more robust phylogenetic framework (Fig. 1) allowed to infer only four independent flagellum losses, plus the ongoing one in sanchytrids (Fig. 3c). Three of them occurred at the base of high-rank taxa: nucleariids, Microsporidia and the

Zoopagomycota+Mucoromycota+Dikarya clade. The fourth loss occurred in *H. curvatum*, an atypical fungus originally classified as a colourless green alga[14] and later reclassified within the Monoblepharidomycota[26,96]. The fourth one concerned *Olpidium,* which our phylogenomic analysis robustly placed as an independent lineage sister to major non-flagellated fungal taxa (Fig. 1b). Although *Olpidium* has a functional flagellum, its flagellar toolkit is reduced, lacking Delta and Epsilon tubulins and several dyneins (Fig. 3c). This suggests that, analogously to sanchytrids, Olpidiomycota represent an intermediate stage between zoosporic fungi possessing fully functional flagella and flagellum–lacking fungi. This would be consistent with observations that Zoopagomycota, the first lineage diverging after Olpidiomycota, possess a degenerated 9+2 microtubular system as potential remnant of the ancestral flagellum[97–99]. Our data support a global scenario of major progressive reduction of the flagellar toolkit from *Olpidium* to Dikarya, with a few additional punctual independent losses or reductions in some distant branches of the fungal tree (*H. curvatum* and sanchytrids). In addition, a putative fifth independent loss in Holomycota might have occurred in the Nephridiophagida, a clade of fungal parasites of insects and myriapods[100,101] without clear affinity with established fungal clades[101]. Recently, a possible relationship to chytrids has been suggested[102]. Genomic or transcriptomic data should clarify their phylogenetic position in the future.

Fungal "vision" and flagellum exaptation

Why do sanchytrids retain a non-motile flagellum with a long kinetosome? Since the primary flagellar function has been lost in favour of amoeboid movement, other selective forces must be acting to retain this atypical structure for a different function in zoospores. In bacteria, the exaptation of the flagellum for new roles in mechanosensitivity[103,104] and wetness sensing[105] has been documented. Microscopy observations of sanchytrid cultures showed that the flagellum is rather labile and can be totally retracted within the cell cytoplasm, the long kinetosome likely being involved in this retraction capability[35,36]. Interestingly, a conspicuous curved rosary chain of lipid globules has been observed in the kinetosome vicinity in *A. gromovi* zoospores, often close to mitochondria[35,36]. In the blastocladiomycete *B. emersonii*, similar structures tightly associated with mitochondria are known as "side-body complexes"[106]. *B. emersonii* possesses a unique bacterial type-1-rhodopsin+guanylyl cyclase domain fusion (BeGC1, 626 amino acids) which, together with a cyclic nucleotide-gated channel (BeCNG1), control zoospore phototaxis in response to cGMP

levels after exposure to green light[107]. BeGC1 was localized by immunofluorescence on the external membrane of the axoneme-associated lipid droplets, which function as an eyespot at the base of the flagellum and control its beating[107–109]. The BeGC1 fusion and the channel BeCNG1 proteins have also been found in other Blastocladiomycota (*A. macrogynus* and *C. anguillulae*).

Both *A. gromovi* and *S. tribonematis* possessed the BeGC1 fusion (532 and 535 amino acids, respectively) and the gated channel BeCNG1 (Supplementary Fig. 12a-c). We also found the BeGC1 fusion in the newly available Blastocladiomycota genome and transcriptome sequences of *P. sedebokerense* and *C. lativittatus*. Therefore, this fusion constitutes a synapomorphy for the Blastocladiomycota+Sanchytriomycota clade. However, we found the BeCNG1 channel in *C. lativittatus* but not in *P. sedebokerense*, suggesting that this species probably uses a different way to finish the cGMP cascade reaction (Supplementary Fig. 12c). Despite some ultrastructural differences, and although functional studies need to confirm their role, the presence of lipid threads in the vicinity of the kinetosome and mitochondria, together with BeGC1/BeCNG1 homologs in *Amoeboradix* and *Sanchytrium* tentatively suggest a comparable light-sensing organelle in sanchytrids. We hypothesize that, as in *B. emersonii,* the sanchytrid reduced flagellum could be involved in phototactic response, at least as an structural support for the lipid vacuoles. Interestingly, sanchytrids showed considerably shorter branches in rhodopsin and guanylyl cyclase domain phylogenetic trees (Supplementary Fig. 12) than in multi-gene phylogenies (Fig. 1), indicating that these proteins (and their functions) are subjected to strong purifying selection as compared to other proteins in their genomes.

Since rhodopsins capture light by using the chromophore retinal[110], we looked for a set of carotenoid (β-carotene) biosynthesis enzymes[107,111] necessary for retinal production. Surprisingly, the enzymes involved in the classical pathway (bifunctional lycopene cyclase/phytoene synthase, phytoene dehydrogenase and carotenoid oxygenase)[107,111] were missing in both sanchytrid genomes, suggesting that they are not capable of synthesize their own retinal (Supplementary Table 4). We only detected two enzymes (isopentenyl diphosphate isomerase and farnesyl diphosphate synthase) that carry out early overlapping steps of both sterol and carotenoid biosynthesis. By contrast, the β-carotene biosynthesis pathway is widely distributed in Fungi, including chytrids and Blastocladiomycota (*Allomyces* and *Blastocladiella*[107,112], and also in *P. sedebokerense* and *C. lativittatus*, Supplementary Table 4). Therefore, sanchytrids, like most heterotrophic eukaryotes, seem unable to synthesize β-carotene and must obtain carotenoids

through their diet[111]. Indeed, we detected all carotenoid and retinal biosynthesis pathway genes in the transcriptome of the yellow-brown alga *Tribonema gayanum,* (Supplementary Table 4), their host and likely retinal source during infection.

Evolution of multicellularity in Holomycota

Fungal multicellularity results from connected hyphae[113]. Diverse genes involved in hyphal multicellularity were present in the ancestors of three lineages of unicellular fungi (Blastocladiomycota, Chytridiomycota and Zoopagomycota; BCZ nodes)[114]. To ascertain whether they were also present in other deep-branching Holomycota with unicellular members, we reconstructed the evolutionary history of 619 hyphal morphogenesis proteins[114], grouped into 10 functional categories (see Methods; Supplementary Table 5; Supplementary Fig. 13). Our results showed that most hyphal morphogenesis genes were not only present in the fungal ancestor but also in their unicellular holomycotan relatives, indicating that they evolved well before the origin of fungal multicellularity (Fig. 4a). This pattern could be observed for all functional categories with the clear exception of the adhesion proteins, most of only occur in Dikarya (Supplementary Fig. 13), reinforcing previous conclusions that adhesion proteins played a marginal role in the early evolution of hyphae[114].

The ancestor of *Olpidium* and the multicellular fungi clade possessed a high percentage of hyphae-related proteins (88.4%, node O in Fig. 4a), similarly to the ancestor of sanchytrids and Blastocladiomycota (82%), though this ancestral repertoire became secondarily reduced in sanchytrids (65.9%). Likewise, many yeasts, which are also secondarily reduced organisms, retained most of the genetic repertoire needed for hyphal development. Many of these proteins were also present in nucleariids, Rozellida-Microsporidia and Aphelida (nodes N, R, and A in Fig. 4a and Supplementary Table 6; NRA nodes). Clustering analysis based on the presence/absence of hyphal morphogenesis proteins did not clearly segregate unicellular and multicellular lineages (Fig. 4b) and retrieved very weak intragroup correlation (Fig. 4c). Our results extend previous observations of hyphal morphogenesis genes from Fungi[114] to much more ancient diversifications in the Holomycota. The holomycotan ancestor already possessed a rich repertoire of proteins, notably involved in 'actin cytoskeleton' and 'microtubule-based transport', that were later recruited for hyphal production (Supplementary Table 6). Most innovation concerned the proteins involved in the 'cell wall biogenesis/remodeling' and 'transcriptional regulation' functional

categories, which expanded since the common ancestor of Aphelida and Fungi. This pattern is consistent with the enrichment of gene duplications in these two categories observed in all major fungal lineages[114]. Nevertheless, genome and transcriptome data remain very scarce for the Aphelida and we expect that part of these duplications will be inferred to be older when more data for this sister lineage of Fungi become available.

Conclusions

We generated the first genome sequence data for the two known species of sanchytrids, a group of atypical fungal parasites of algae. The phylogenetic analysis of 264 conserved proteins showed that they form a new fungal phylum, the Sanchytriomycota, sister to the Blastocladiomycota. Our phylogenetic analysis also provided strong support for Chytridiomycota being the sister group of all other fungi and confirmed the position of the enigmatic flagellated fungus *Olpidium* as sister of the main group of non-flagellated fungi (Zoopagomycota+Mucoromycota+Dikarya). Sanchytrids have a complex life cycle that includes a flagellated phase (zoospores) with non-motile flagella that are engaged in an ongoing reductive process. The inclusion of both, other zoosporic (e.g., *Olpidium*) and non-flagellated (e.g., the chytrid *H. curvatum*), fungi in our multi-gene phylogeny allowed the inference of four independent flagellum losses across Holomycota. Interestingly, the sanchytrid residual flagellum endowed with a long kinetosome might represent an exaptation of this structure as support for a lipid organelle putatively involved in light sensing. Our taxon-rich dataset of deep-branching Holomycota also provided evidence for a very ancient origin of most genes related to hyphal morphogenesis, well before the evolution of the multicellular fungal lineages.

Taxonomic appendix

Sanchytriomycota phyl. nov.

Monocentric thallus, epibiotic; usually amoeboid zoospores with longest-known kinetosome in fungi and immobile pseudocilium; centrosome in sporangium with two centrioles composed by nine microtubular singlets.

Class **Sanchytriomycetes** (Tedersoo et al. 2018)[34] emend.

Diagnosis as for the phylum.

411 Order **Sanchytriales** (Tedersoo et al. 2018)[34] emend.

412 Diagnosis as for the phylum.

413 Family **Sanchytriaceae** (Karpov & Aleoshin, 2017)[45] emend.

414 Amoeboid zoospores with anterior lamellipodium producing subfilopodia, and lateral and
415 posterior filopodia; with (rarely without) posterior pseudocilium; kinetosome composed of nine
416 microtubule singlets or singlets/doublets, 1–2 μm in length. Zoospores attach to algal cell wall,
417 encyst, and penetrate host wall with a short rhizoid. Interphase nuclei in sporangia have a
418 centrosome of two centrioles composed of nine microtubular singlets. Predominantly parasites of
419 freshwater algae.

420 Type: **Sanchytrium** (Karpov et Aleoshin 2017[45]) emend. Karpov, 2019[36].

421 Parasite of algae. Epibiotic, spherical to ovate, sporangia with one (rarely more) discharge papillae.
422 Amoeboid zoospores with anterior lamellipodium; with (rarely without) pseudocilium; contains
423 kinetosome composed of nine single microtubules 1–1.2 μm in length. Interphase nuclei in
424 sporangia have a centrosome with two orthogonal centrioles composed of nine microtubular
425 singlets and with an internal fibrillar ring.

426 Type: *Sanchytrium tribonematis* (Karpov et Aleoshin, 2017[45]) emend. Karpov, 2019[36].

427 ***Sanchytrium tribonematis*** (Karpov et Aleoshin, 2017[45]) emend. Karpov, 2019[36].

428 Round to ovate smooth sporangium, ~10 μm diameter, without or with one discharge papilla;
429 sessile on algal surface. Slightly branched rhizoid, almost invisible inside host. Amoeboid
430 zoospores 5.4 - 3.3 μm (maximum) with anterior lamellipodium producing subfilopodia, lateral
431 and posterior filopodia; normally with posterior pseudocilium up to 5 μm in length supported by
432 up to four microtubules.

433 ***Amoeboradix*** Karpov, López-García, Mamkaeva & Moreira, 2018[35].

434 Zoosporic fungus with monocentric, epibiotic sporangia and amoeboid zoospores having posterior
435 pseudocilium that emerges from long kinetosome (ca. 2 μm) composed of microtubular singlets
436 or doublets.

437 Type species: *A. gromovi* Karpov, López-García, Mamkaeva & Moreira, 2018[35].

438 ***A. gromovi*** Karpov, López-García, Mamkaeva & Moreira, 2018[35].

439 Amoeboid zoospores of 2-3×3-4 µm with posterior pseudocilium up to 8 µm in length, which can
440 be totally reduced; kinetosome length, 1.8-2.2 µm. Sporangia of variable shape, from pear-shaped
441 with rounded broad distal end and pointed proximal end to curved asymmetrical sac-like 8-10 µm
442 width 16-18 µm long with prominent rhizoid and 2-3 papillae for zoospore discharge; spherical
443 cysts about 3-4 µm in diameter; resting spore is ovate thick walled 12×6 µm. Parasite of *Tribonema*
444 *gayanum, T. vulgare* and *Ulothrix tenerrima.*

445

446 **Methods**

447 **Biological material.** *Sanchytrium tribonematis* strain X-128 and *Amoeboradix gromovi* strain X-
448 113, isolated from freshwater sampling locations in Russia[35,36], were maintained in culture with
449 the freshwater yellow-green alga *Tribonema gayanum* Pasch. strain 20 CALU as host [45]. The algal
450 host was grown in mineral freshwater medium at room temperature under white light. After
451 inoculation with *Sanchytrium* or *Amoeboradix*, cultures were incubated for 1–2 weeks to reach the
452 maximum infection level. We then collected both individual zoospores and sporangia full of
453 moving zoospores by micromanipulation with an Eppendorf PatchMan NP2 micromanipulator
454 using 19 µm VacuTip microcapillaries (Eppendorf) on an inverted Leica Dlll3000 B microscope.
455 Zoospores and sporangia were then washed 2 times in clean sterile water drops before storing them
456 into individual tubes for further analyses.

457

458 **Whole genome amplification and sequencing.** DNA extraction from single zoospores and
459 sporangia was done with the PicoPure kit (Thermo Fisher Scientific) according to the
460 manufacturer's protocol. Whole genome amplification (WGA) was carried out by multiple
461 displacement amplification with the single-cell REPLI-g kit (QIAGEN). DNA amplification was
462 quantified using a Qubit fluorometer (Life Technologies). We retained WGA products that yielded
463 high DNA concentration and for which we were able to obtain sanchytrid 18S rRNA gene
464 amplicons by PCR. As expected, WGA from sporangia (many zoospores per sporangium) yielded
465 more DNA than individual zoospores and were selected for sequencing (K1-9_WGA for *A.*
466 *gromovi*; SC-2_WGA for *S. tribonematis*). TruSeq paired-end single-cell libraries were prepared
467 from these samples and sequenced on a HiSeq 2500 Illumina instrument (2 x 100 bp) with v4

chemistry. We obtained 121,233,342 reads (26,245 Mbp) for *A. gromovi* and 106,922,235 reads (21,384 Mbp) for *S. tribonematis*.

Genome sequence assembly, decontamination and annotation. Paired-end read quality was assessed with FastQC[115] before and after quality trimming. Illumina adapters were removed with Trimmomatic v0.32 in Paired-End mode[116], with the following parameters: ILLUMINACLIP:adapters.fasta:2:30:10LEADING:28 TRAILING:28 SLIDINGWINDOW:4:30. Trimmed paired-end reads were assembled using SPAdes 3.9.1 in single-cell mode[117]. This produced assemblies of 48.7 and 37.1 Mb with 8,420 and 8,015 contigs for *A. gromovi* and *S. tribonematis*, respectively. The decontamination of contaminant prokaryotic contigs was carried out by a three-step process. First, genome sequences were subjected to two rounds of assembly, before and after bacterial sequence removal with BlobTools v0.9.19[118]. Second, open-reading frames were predicted and translated from the assembled contigs using Transdecoder v2 (http:transdecoder.github.io) with default parameters and Cd-hit v4.6[119] with 100% identity to produce protein sequences for *A. gromovi* and *S. tribonematis*. Finally, to remove possible eukaryotic host (*Tribonema*) contamination, the predicted protein sequences were searched by BLASTp[120] against two predicted yellow-green algae proteomes inferred from the *Tribonema gayanum* transcriptome [13] and the *Heterococcus* sp. DN1 genome (PRJNA210954) (also member of the Tribonematales). We excluded sanchytrid hits that were 100% or >95% identical to them, respectively. Statistics of the final assembled genomes were assessed with QUAST 4.5[121] and Qualimap v2.2.1[122] for coverage estimation. In total, we obtained 7,220 and 9,368 protein sequences for *A. gromovi* and *S. tribonematis*, respectively (Table 1). To assess genome completeness, we used BUSCO v2.0.1[40] on the decontaminated predicted proteomes with the fungi_odb9 dataset of 290 near-universal single-copy orthologs. The inferred proteins were functionally annotated with eggNOG mapper[72] using DIAMOND as the mapping mode and the eukaryotic taxonomic scope. This resulted in 3,757 (*A. gromovi*) and 4,670 (*S. tribonematis*) functionally annotated peptides for the predicted proteomes (Supplementary Table 1). The mitochondrial genomes of both sanchytrids were identified in single contigs using Blast[123] and annotated with MITOS[124]. Additional Blast searches were made to confirm missing proteins.

Phylogenomic analyses and single-gene phylogenies. A revised version of a 264 protein dataset (termed GBE)[47] was used to reconstruct phylogenomic trees[13,51]. This dataset was updated with sequences from the two sanchytrid genomes, the non-flagellated chytrid *Hyaloraphidium curvatum* SAG235-1 (SRX4387575), the enigmatic flagellated fungus *Olpidium bornovanus* UBC F19785 (SRX125102, SRX123912, SRX123911), and all publicly available Blastocladiomycota sequences, including the recently sequenced *Paraphysoderma sadebokerense* JEL821 (SRX3538887) and *Coelomomyces lativittatus* ClRM-AVA-1 (SRX2781572). Sequences were obtained from GenBank (http://www.ncbi.nlm.nih.gov/genbank, last accessed November, 2019), and the Joint Genome Institute (http://www.jgi.doe.gov/; last accessed May 2017). Our updated taxon sampling comprises a total of 81 Opisthokonta (2 Holozoa and 79 Holomycota), 2 Amoebozoa and 1 Apusomonadida. Two datasets with two different taxon samplings were prepared, one with all 84 species (GBE84) and one without the long-branching core Microsporidia and metchnikovellids for a total of 69 species (GBE69).

The 264 proteins were searched in the new species with tBLASTn[120], incorporated into the individual protein datasets, aligned with MAFFTv7 [125] and trimmed with TrimAl with the automated1 option[126]. Alignments were visualized, manually edited and concatenated with Geneious v6.0.6[127] and single gene trees obtained with FastTree v2.1.7[128] with default parameters. Single gene trees were manually checked to identify and remove paralogous and/or contaminating sequences. The concatenation of the clean trimmed 264 proteins resulted in alignments containing 91,768 (GBE69) and 83,321 (GBE84) amino acid positions. Bayesian inference (BI) phylogenetic trees were reconstructed using PhyloBayes-MPI v1.5[129] under CAT-Poisson model, two MCMC chains for each dataset were run for more than 15,000 generations, saving one every 10 trees. Analyses were stopped once convergence thresholds were reached (i.e. maximum discrepancy <0.1 and minimum effective size >100, calculated using bpcomp) and consensus trees constructed after a burn-in of 25%. Maximum likelihood (ML) phylogenetic trees were inferred with IQ-TREE v1.6[130] under the LG + R9 + PMSF model for GBE69 and LG + F+ R10 + PMSF for GBE84, selected with the IQ-TREE TESTNEW algorithm as per the Bayesian information criterion (BIC). Statistical support was generated with 1000 ultrafast bootstraps[131] and 1,000 replicates of the SH-like approximate likelihood ratio test[132]. All trees were visualized with FigTree[133].

To test alternative tree topologies we used Mesquite[134] to constrain the following topologies: 1) chytrids as sister lineage of all other fungi (Blastocladiomycota + Sanchytriomycota

529 + *Olpidium* + Zygomycota + Dikarya), 2) Blastocladiomycota + Sanchytriomycota as sister
530 lineage of all other fungi (Chytridiomycota + *Olpidium* + Zygomycota + Dikarya), and 3)
531 *Olpidium* as an independent lineage sister of all other non-flagellated fungi (Zygomycota +
532 Dikarya) or belonging within Zoopagomycota. The constrained topologies without branch lengths
533 were reanalysed with the -g option of IQ-TREE and the best-fitting model. AU tests were carried
534 out on the resulting trees for each taxon sampling with the -z and -au options of IQ-TREE.
535 Additionally, to minimize possible systematic bias due to the inclusion of fast-evolving sites in
536 our protein alignments, we progressively removed the fastest evolving sites, 5% of sites at a time.
537 For that, among-site substitution rates were inferred using IQ-TREE under the -wsr option and the
538 best-fitting model for both taxon samplings for a total of 19 new data subsets of each
539 (Supplementary Table 2). We then reconstructed phylogenetic trees for all these subsets using IQ-
540 TREE with the same best-fitting model as for the whole dataset. To assess the support of the
541 alternative topologies in the bootstrapped trees, we used CONSENSE from the PHYLIP
542 package[135] and interrogated the UFBOOT file using a Python script (M. Kolisko, pers. comm).
543 Finally, to remove possible compositional heterogeneity within our data, we used the Dayhoff
544 recoding scheme (from 20 to 4 categories) using an in-house Python script. We then reconstructed
545 phylogenetic trees for all the recoded subsets using IQ-TREE with the GTR+F+I+G4 model for
546 ML trees and PhyloBayes-MPI v1.5 with the CAT-Poisson model for BI trees.
547
548 **Comparative analysis of primary metabolism.** To get insights into the metabolic capabilities of
549 sanchytrids in comparison with other Holomycota we carried out statistical multivariate analyses.
550 Protein sets used in this study were obtained between May 2017 and November 2019 from the
551 NCBI protein, genome and SRA databases (https://www.ncbi.nlm.nih.gov/), except the following:
552 *Spizellomyces punctatus*, *Gonapodya prolifera*, *Batrachochytrium dendrobatidis*, *Allomyces*
553 *macrogynus*, *Catenaria anguillulae* and *Blastocladiella britannica*, retrieved from the MycoCosm
554 portal of the Joint Genome Institute (these sequence data were produced by the US Department of
555 Energy Joint Genome Institute http://www.jgi.doe.gov/ in collaboration with the user community)
556 and *Parvularia atlantis* (previously *Nuclearia* sp. ATCC50694, from
557 https://doi.org/10.6084/m9.figshare.3898485.v4). We searched in both sanchytrids 1206 eggNOG
558 orthologous groups[72] corresponding to 8 primary metabolism categories (Gene Ontology, GO).
559 The correspondence between GO terms and primary metabolism COGs used are the following:

[C] Energy production and conversion (227 orthologs); [G] Carbohydrate transport and metabolism (205 orthologs); [E] Amino acid transport and metabolism (200 orthologs); [F] Nucleotide transport and metabolism (87 orthologs); [H] Coenzyme transport and metabolism (94 orthologs); [I] Lipid transport and metabolism (201 orthologs); [P] Inorganic ion transport and metabolism (153 orthologs); and [Q] Secondary metabolites biosynthesis, transport and catabolism (70 orthologs). From these categories, we identified 1158 orthologs non-redundant among categories in the sanchytrid genomes which were shared among a set of 45 species, including 8 opisthosporidians, 30 fungi, 2 holozoans, 2 amoebozoans, and 1 apusomonad (for the complete list, see Supplementary Table 3). We annotated the protein sets of these 45 species using eggNOG-mapper[72] with DIAMOND as mapping mode and the eukaryotic taxonomic scope. All ortholog counts were transformed into a presence/absence matrix (encoded as 0/1) and analysed with the R script[136] detailed in Torruella et al. (2018) in which similarity values between binary COG profiles of all species were calculated to create a complementary species-distance matrix. We then analysed this distance matrix using a Principal Coordinate Analysis (PCoA) and plotted binary COG profiles in a presence/absence heatmap. Clustering of the species and orthologs was done by Ward hierarchical clustering (on Euclidean distances for orthologs) of the interspecific Pearson correlation coefficients. The raw species clustering was also represented in a separate pairwise correlation heatmap colour-coded to display positive Pearson correlation values (0–1). Finally, COG categories of each primary metabolism were also analysed separately (categories C, E, F, G, H, I, P, and Q) using the same workflow (for more details see Torruella et al. 2018 and https://github.com/xgrau/paraphelidium2018). We compared in more detail the inferred metabolism of a subset of species (the two sanchytrids, *Rozella allomycis* and *Allomyces macrogynus*). The annotation of these proteomes was done using BlastKOALA[137], with eukaryotes as taxonomy group and the genus_eukaryotes KEGG GENES database, and the annotations uploaded in the KEGG Mapper Reconstruct Pathway platform[79] by pairs. First, we compared the two sanchytrid proteomes to confirm their similarity and, second, we compared them with the proteomes of *R. allomycis* and *A. macrogynus* to study their metabolic reduction.

Homology searches and phylogenetic analysis of specific proteins. To assess the evolution of the flagellum in holomycotan lineages we used a dataset of over 60 flagellum-specific proteins [85,138–140] to examine a total of 47 flagellated and non-flagellated species within and outside the

Holomycota. The flagellar toolkit proteins were identified using *Homo sapiens* sequences as Blast queries. Candidate proteins were then blasted against the non-redundant GenBank database to confirm their identification and submitted to phylogenetic analysis by multiple sequence alignment with MAFFT[125], trimming with TrimAl[126] with the automated1 option, and tree reconstruction with FastTree[128]. After inspection of trees, we removed paralogs and other non-orthologous protein sequences. We excluded the proteins with no identifiable presence in any of the 47 species used in the analysis and encoded the presence/absence of the remaining ones in a 1/0 matrix. The native R heatmap function[136] was used to plot the flagellar proteome comparison between all species according to their presence/absence similarity profiles. To study the presence or absence of the fusion of the BeGC1 and BeCNG1 light-sensing proteins, we blasted them against the proteomes of *S. tribonematis*, *A. gromovi*, *P. sedebokerense* and *C. lativittatus* using the *Blastocladiella emersonii* sequences (BeGC1: AIC07007.1; BeCNG1: AIC07008.1) as queries. We used MAFFT to include the new sequences in a multiple sequence alignment for the BeCNG1 protein channel and separately for both the guanylyl-cyclase GC1 domain and the rhodopsin domain of the BeGC1 fusion protein[107]. After trimming with TrimAl we reconstructed phylogenetic trees for the three datasets using IQ-TREE with the best-fitting models: LG+F+I+G4 for the rhodopsin domain and BeCNG1, and LG+G4 model for BeGC1. The resulting trees were visualized with FigTree[133]. To study the possible presence of a carotenoid synthesis pathway for retinal production in sanchytrids, we combined previous datasets for carotenoid biosynthesis and cleavage enzymes from one giant virus (ChoanoV1), two choanoflagellates and two haptophytes[111], together with the carotenoid biosynthesis enzymes found in *B. emersonii*[107]. This dataset also included three enzymes for early sterol and carotenoid biosynthesis (isoprenoid biosynthesis steps). The protein sequences from this dataset where blasted (BLASTp) against the two sanchytrid proteomes and their host *Tribonema gayanum* proteome. Results were confirmed by blasting the identified hits to the NCBI non-redundant protein sequence database. To study the presence of proteins involved in cell-wall penetration in sanchytrids (including cellulases, hemicellulases chitinases and pectinases), we used the complete mycoCLAP database of carbohydrate-degrading enzymes (https://mycoclap.fungalgenomics.ca/mycoCLAP/). We blasted this database against our two sanchytrid proteomes and other five close representatives of Blastocladiomycota and four Chytridiomycota. We then screened for canonical cellulose, hemicellulose, pectin and chitin degrading enzymes identified in Fungi from previous studies[13,141,142]. The identified hits were

blasted back to both the NCBI non-redundant protein sequence database and the CAZy database (cazy.org) to create a dataset for phylogenetic reconstruction for each enzyme. In some cases, we added the identified sequences to specific protein datasets from previous studies. For cellulases, we updated a previous aphelid dataset[13], and for the chitin degradation proteins we updated previous datasets of GH20 β -N-acetylhexosaminidase (NAGase)[83] and GH18 chitinase[82]. Proteins were aligned with MAFFT[125] and trimmed from gaps and ambiguously aligned sites using TrimAl[126] with the automated1 algorithm. ML trees were inferred using IQ-TREE[130] with the best-fitting model selected with the IQ-TREE TESTNEW algorithm as per BIC. The best-scoring tree was searched for up to 100 iterations, starting from 100 initial parsimonious trees; statistical supports were generated from 1000 ultra-fast bootstrap replicates and 1000 replicates of the SH-like approximate likelihood ratio test. Trees were visualized with FigTree[133].

Analyses of hyphae multicellularity-related genes. We used a dataset of 619 hyphal multicellularity-related proteins belonging to 362 gene families[114]. These gene families were grouped into 10 functional categories: actin cytoskeleton (55 proteins), adhesion (30), polarity maintenance (107), cell wall biogenesis/remodeling (92), septation (56), signaling (82), transcriptional regulation (51), vesicle transport (103), microtubule-based transport (32) and cell cycle regulation (11). The 619 proteins were searched by BLAST in the GBE69 dataset proteome and later incorporated into individual gene family protein alignments with MAFFT v7[125]. After trimming with TrimAl[126] with the automated1 option, alignments were visualized with Geneious v6.0.6[127] and single gene trees obtained with FastTree[128] with default parameters. Single protein trees were manually checked to identify paralogous sequences and confirm the presence of genes within large gene families. Presence/absence of genes was binary coded (0/1) for each species and the resulting matrix processed with a specific R script[13]. Finally, we reconstructed the multicellularity-related gene gain/loss dynamics by applying the Dollo parsimony method implemented in Count[143]. These analyses were done on both the complete dataset of all hyphae multicellularity-related genes and on 10 separate datasets corresponding to the functional categories mentioned above.

Data availability

652 The raw sequence data and assembled genomes generated in this work have been deposited at the
653 National Center for Biotechnology Information (NCBI) sequence databases under Bioprojects
654 PRJNA668693 and PRJNA668694.
655
656 **Acknowledgments**
657 We thank the UNICELL single-cell genomics platform (https://www.deemteam.fr/en/unicell).
658 This work was funded by the European Research Council Advanced Grants "ProtistWorld" (No.
659 322669, P.L.-G.) and Plast-Evol (No. 787904, D.M.) and the Horizon 2020 research and
660 innovation program under the Marie Skłodowska-Curie ITN project SINGEK
661 (http://www.singek.eu/; grant agreement No. H2020-MSCA-ITN-2015-675752, L.J.G. & P.L.-
662 G.). S.A.K. contribution was supported by the RSF grant No. 16-14-10302.
663
664 **Author contributions**
665 P.L.-G. and D.M. conceived and supervised the study. S.A.K. and D.M. prepared the biological
666 material; L.J.G., G.T. and D.M. analysed the sequence data; L.J.G., P.L.-G. and D.M. supervised
667 the study and wrote the manuscript, which was edited and approved by all authors.
668
669 **Competing interests**
670 The authors declare no competing interests.
671
672 **Correspondence and requests for materials** should be addressed to L.J.G or D.M.
673
674 **References**
675 1. Cavalier-Smith, T. A revised six-kingdom system of life. *Biol. Rev. Camb. Philos. Soc.* **73**, 203–266
676 (1998).
677 2. Douzery, E. J. P., Snell, E. A., Bapteste, E., Delsuc, F. & Philippe, H. The timing of eukaryotic
678 evolution: Does a relaxed molecular clock reconcile proteins and fossils? *Proc. Natl. Acad. Sci. U.*
679 *S. A.* (2004) doi:10.1073/pnas.0403984101.
680 3. Parfrey, L. W., Lahr, D. J. G., Knoll, A. H. & Katz, L. A. Estimating the timing of early eukaryotic
681 diversification with multigene molecular clocks. *Proc. Natl. Acad. Sci. U. S. A.* (2011)
682 doi:10.1073/pnas.1110633108.
683 4. Eme, L., Sharpe, S. C., Brown, M. W. & Roger, A. J. On the age of eukaryotes: Evaluating evidence

from fossils and molecular clocks. *Cold Spring Harb. Perspect. Biol.* **6**, 1–16 (2014).

5. Berbee, M. L., James, T. Y. & Strullu-Derrien, C. Early diverging fungi: Diversity and impact at the dawn of terrestrial life. *Annu. Rev. Microbiol.* **71**, 41–60 (2017).
6. Spatafora, J. W. *et al.* The Fungal Tree of Life: from molecular systematics to genome-scale phylogenies. *Microbiol. Spectr.* **5**, 1–32 (2017).
7. Lara, E., Moreira, D. & López-García, P. The environmental clade LKM11 and *Rozella* form the deepest branching clade of Fungi. *Protist* **161**, 116–121 (2010).
8. Jones, M. D. M. *et al.* Discovery of novel intermediate forms redefines the fungal tree of life. *Nature* (2011) doi:10.1038/nature09984.
9. James, T. Y. *et al.* Shared signatures of parasitism and phylogenomics unite cryptomycota and microsporidia. *Curr. Biol.* **23**, 1548–1553 (2013).
10. Karpov, S. A. *et al.* Morphology, phylogeny, and ecology of the aphelids (Aphelidea, Opisthokonta) and proposal for the new superphylum Opisthosporidia. *Frontiers in Microbiology* (2014) doi:10.3389/fmicb.2014.00112.
11. Haag, K. L. *et al.* Evolution of a morphological novelty occurred before genome compaction in a lineage of extreme parasites. *Proc. Natl. Acad. Sci.* **111**, 15480–15485 (2014).
12. Bass, D. *et al.* Clarifying the Relationships between Microsporidia and Cryptomycota. *J. Eukaryot. Microbiol.* **65**, 773–782 (2018).
13. Torruella, G. *et al.* Global transcriptome analysis of the aphelid *Paraphelidium tribonemae* supports the phagotrophic origin of fungi. *Commun. Biol.* **1**, 1–11 (2018).
14. Ustinova, I., Krienitz, L. & Huss, V. A. R. *Hyaloraphidium curvatum* is not a green alga but a lower fungus; *Amoebidium parasiticum* is not a fungus, but a member of the DRIPs. *Protist* (2000) doi:10.1078/1434-4610-00023.
15. Powell, M. J. Looking at mycology with a Janus face: a glimpse at Chytridiomycetes active in the environment. *Mycologia* (1993) doi:10.2307/3760471.
16. Freeman, K. R. *et al.* Evidence that chytrids dominate fungal communities in high-elevation soils. *Proc. Natl. Acad. Sci. U. S. A.* (2009) doi:10.1073/pnas.0907303106.
17. Kagami, M., Miki, T. & Takimoto, G. Mycoloop: Chytrids in aquatic food webs. *Front. Microbiol.* (2014) doi:10.3389/fmicb.2014.00166.
18. Frenken, T. *et al.* Warming accelerates termination of a phytoplankton spring bloom by fungal parasites. *Glob. Chang. Biol.* (2016) doi:10.1111/gcb.13095.
19. Frenken, T. *et al.* Integrating chytrid fungal parasites into plankton ecology: research gaps and needs. *Environmental Microbiology* (2017) doi:10.1111/1462-2920.13827.
20. Tedersoo, L., Bahram, M., Puusepp, R., Nilsson, R. H. & James, T. Y. Novel soil-inhabiting clades

fill gaps in the fungal tree of life. *Microbiome* (2017) doi:10.1186/s40168-017-0259-5.

21. James, T. Y. *et al.* A molecular phylogeny of the flagellated fungi (Chytridiomycota) and description of a new phylum (Blastocladiomycota). *Mycologia* **98**, 860–871 (2006).
22. Chang, Y. *et al.* Phylogenomic analyses indicate that early fungi evolved digesting cell walls of algal ancestors of land plants. *Genome Biol. Evol.* **7**, 1590–1601 (2015).
23. Liu, Y. J., Hodson, M. C. & Hall, B. D. Loss of the flagellum happened only once in the fungal lineage: Phylogenetic structure of Kingdom Fungi inferred from RNA polymerase II subunit genes. *BMC Evol. Biol.* **6**, 1–13 (2006).
24. Bidartondo, M. I. *et al.* The dawn of symbiosis between plants and fungi. *Biol. Lett.* (2011) doi:10.1098/rsbl.2010.1203.
25. Lutzoni, F. *et al.* Contemporaneous radiations of fungi and plants linked to symbiosis. *Nat. Commun.* **9**, 1–11 (2018).
26. Sekimoto, S., Rochon, D., Long, J. E., Dee, J. M. & Berbee, M. L. A multigene phylogeny of *Olpidium* and its implications for early fungal evolution. *BMC Evol. Biol.* **11**, 331 (2011).
27. Spatafora, J. W. *et al.* A phylum-level phylogenetic classification of zygomycete fungi based on genome-scale data. *Mycologia* **108**, 1028–1046 (2016).
28. Taylor, J. W. & Berbee, M. L. Dating divergences in the Fungal Tree of Life: Review and new analyses. *Mycologia* (2006) doi:10.3852/mycologia.98.6.838.
29. Loron, C. C. *et al.* Early fungi from the Proterozoic era in Arctic Canada. *Nature* (2019) doi:10.1038/s41586-019-1217-0.
30. Ebersberger, I. *et al.* A consistent phylogenetic backbone for the fungi. *Mol. Biol. Evol.* **29**, 1319–1334 (2012).
31. James, T. Y. *et al.* Reconstructing the early evolution of Fungi using a six-gene phylogeny. *Nature* **443**, 818–822 (2006).
32. Barr, D. J. S. An outline for the reclassification of the Chytridiales, and for a new order, the Spizellomycetales. *Can. J. Bot.* **58**, 2380–2394 (1980).
33. Powell, M. J. & Letcher, P. M. Chytridiomycota, Monoblepharidomycota, and Neocallimastigomycota. in *Systematics and Evolution: Part A: Second Edition* (2014). doi:10.1007/978-3-642-55318-9.
34. Tedersoo, L. *et al.* High-level classification of the Fungi and a tool for evolutionary ecological analyses. *Fungal Divers.* **90**, 135–159 (2018).
35. Karpov, S. A. *et al.* The Chytrid-like Parasites of algae *Amoeboradix gromovi* gen. et sp. nov. and *Sanchytrium tribonematis* belong to a new fungal lineage. *Protist* **169**, 122–140 (2018).
36. Karpov, S. A., Vishnyakov, A. E., Moreira, D. & López-García, P. The ultrastructure of *Sanchytrium*

tribonematis (Sanchytriaceae, Fungi incertae sedis) confirms its close relationship to *Amoeboradix*. *J. Eukaryot. Microbiol.* 0–2 (2019) doi:10.1111/jeu.12740.

37. McCarthy, C. G. P. & Fitzpatrick, D. A. *Multiple Approaches to Phylogenomic Reconstruction of the Fungal Kingdom*. *Advances in Genetics* vol. 100 (Elsevier Inc., 2017).

38. Ahrendt, S. R. *et al.* Leveraging single-cell genomics to expand the fungal tree of life. *Nat. Microbiol.* **3**, 1417–1428 (2018).

39. Li, Y. *et al.* A genome-scale phylogeny of Fungi; insights into early evolution, radiations, and the relationship between taxonomy and phylogeny. *bioRxiv* (2020) doi:10.1101/2020.08.23.262857.

40. Simão, F. A., Waterhouse, R. M., Ioannidis, P., Kriventseva, E. V. & Zdobnov, E. M. BUSCO: Assessing genome assembly and annotation completeness with single-copy orthologs. *Bioinformatics* **31**, 3210–3212 (2015).

41. Billon-Grand, G., Fiol, J. B., Breton, A., Bruyère, A. & Oulhaj, Z. DNA of some anaerobic rumen fungi: G + C content determination. *FEMS Microbiol. Lett.* (1991) doi:10.1111/j.1574-6968.1991.tb04893.x.

42. Youssef, N. H. *et al.* The genome of the anaerobic fungus *Orpinomyces* sp. strain c1a reveals the unique evolutionary history of a remarkable plant biomass degrader. *Appl. Environ. Microbiol.* (2013) doi:10.1128/AEM.00821-13.

43. Videvall, E. *Plasmodium* parasites of birds have the most AT-rich genes of eukaryotes. *Microb. genomics* **4**, (2018).

44. Chen, Y. ping *et al.* Genome sequencing and comparative genomics of honey bee microsporidia, *Nosema apis* reveal novel insights into host-parasite interactions. *BMC Genomics* (2013) doi:10.1186/1471-2164-14-451.

45. Karpov, S. A. *et al.* Monoblepharidomycetes diversity includes new parasitic and saprotrophic species with highly intronized rDNA. *Fungal Biol.* **121**, 729–741 (2017).

46. Thomarat, F., Vivarès, C. P. & Gouy, M. Phylogenetic analysis of the complete genome sequence of *Encephalitozoon cuniculi* supports the fungal origin of microsporidia and reveals a high frequency of fast-evolving genes. *J. Mol. Evol.* **59**, 780–791 (2004).

47. Mikhailov, K. V, Simdyanov, T. G., Aleoshin, V. V & Belozersky, A. N. Genomic survey of a hyperparasitic microsporidian *Amphiamblys* sp. (Metchnikovellidae) *Genome Biology and Evolution* (2016) doi:10.1093/gbe/evw235.

48. Galindo, L. J. *et al.* Evolutionary genomics of *Metchnikovella incurvata* (metchnikovellidae): An early branching microsporidium. *Genome Biol. Evol.* **10**, 2736–2748 (2018).

49. Aguileta, G. *et al.* High variability of mitochondrial gene order among fungi. *Genome Biol. Evol.* (2014) doi:10.1093/gbe/evu028.

50. Mikhailov, K. V., Simdyanov, T. G. & Aleoshin, V. V. Genomic survey of a hyperparasitic microsporidian *Amphiamblys* sp. (Metchnikovellidae). *Genome Biol. Evol.* (2017) doi:10.1093/gbe/evw235.

51. Galindo, L. J. *et al.* Combined cultivation and single-cell approaches to the phylogenomics of nucleariid amoebae, close relatives of fungi. *Philos. Trans. R. Soc. B Biol. Sci.* **374**, 20190094 (2019).

52. Lartillot, N. & Philippe, H. A Bayesian mixture model for across-site heterogeneities in the amino-acid replacement process. *Mol. Biol. Evol.* **21**, 1095–1109 (2004).

53. Wang, H. C., Minh, B. Q., Susko, E. & Roger, A. J. Modeling site heterogeneity with posterior mean site frequency profiles accelerates accurate phylogenomic estimation. *Syst. Biol.* (2018) doi:10.1093/sysbio/syx068.

54. Hoffman, Y. *et al.* Isolation and characterization of a novel chytrid species (phylum Blastocladiomycota), parasitic on the green alga *Haematococcus*. *Mycol. Res.* (2008) doi:10.1016/j.mycres.2007.09.002.

55. Gutman, J., Zarka, A. & Boussiba, S. The host-range of *Paraphysoderma sedebokerensis*, a chytrid that infects *Haematococcus pluvialis*. *Eur. J. Phycol.* (2009) doi:10.1080/09670260903161024.

56. James, T. Y., Hoffman, Y., Zarka, A. & Boussiba, S. *Paraphysoderma sedebokerense*, gen. et sp. Nov., an aplanosporic relative of *Physoderma* (Blastocladiomycota). *Mycotaxon* (2011) doi:10.5248/118.177.

57. Couch, J. N. Validation of the family Coelomomycetaceae and certain species and varieties of *Coelomomyces*. *J. Elisha Mitchell Sci. Soc.* **78**, 135–138 (1962).

58. Uebelmesser, E. ruth. Über einige neue Chytridineen aus Erdboden - *Olpidium, Rhizophidium, Phlyctochytrium* und *Rhizophlyctis*. *Arch. Mikrobiol.* (1956) doi:10.1007/BF00424866.

59. Leipe, D. D., GUNDERSON, J. H., Nerad, T. A. & Sogin, M. L. Small subunit ribosomal rna of *Hexamita inflata* and the quest for the 1st branch in the eukaryotic tree. *Molecular Biochemical Parasitology* vol. 59 41–48 (1993).

60. Kamaishi, T. *et al.* Complete Nucleotide sequences of the genes encoding translation elongation factors 1 and 2 from a microsporidian parasite, *Glugea plecoglossi*: Implications for the deepest branching of eukaryotes. *J. Biochem.* **120**, 1095–1103 (1996).

61. Philippe, H. *et al.* Early-branching or fast-evolving eukaryotes? An answer based on slowly evolving positions. *Proc. R. Soc. B Biol. Sci.* **267**, 1213–1221 (2000).

62. Brinkmann, H. & Philippe, H. Archaea sister group of Bacteria? Indications from tree reconstruction artifacts in ancient phylogenies. *Mol. Biol. Evol.* (1999) doi:10.1093/oxfordjournals.molbev.a026166.

63. Susko, E. & Roger, A. J. On reduced amino acid alphabets for phylogenetic inference. *Mol. Biol. Evol.* (2007) doi:10.1093/molbev/msm144.

64. Olive, L. S. *Caulochytrium protostelioides* sp. nov., a new chytrid with aerial sporangia. *Am. J. Bot.* (1980) doi:10.2307/2442298.

65. Chang, Y. *et al.* Genome-scale phylogenetic analyses confirm *Olpidium* as the closest living zoosporic fungus to the non-flagellated, terrestrial fungi. *bioRxiv* (2020) doi:10.1101/2020.09.16.298935.

66. Naranjo-Ortiz, M. A. & Gabaldón, T. Fungal evolution: diversity, taxonomy and phylogeny of the Fungi. *Biol. Rev.* **94**, 2101–2137 (2019).

67. Field, K. J. *et al.* First evidence of mutualism between ancient plant lineages (Haplomitriopsida liverworts) and Mucoromycotina fungi and its response to simulated Palaeozoic changes in atmospheric CO2. *New Phytol.* (2015) doi:10.1111/nph.13024.

68. Feijen, F. A. A., Vos, R. A., Nuytinck, J. & Merckx, V. S. F. T. Evolutionary dynamics of mycorrhizal symbiosis in land plant diversification. *Sci. Rep.* (2018) doi:10.1038/s41598-018-28920-x.

69. Vargas, M. M., Aronson, J. M. & Roberson, R. W. The cytoplasmic organization of hyphal tip cells in the fungus *Allomyces macrogynus*. *Protoplasma* (1993) doi:10.1007/BF01378938.

70. Stajich, J. E. *et al.* The Fungi. *Current Biology* (2009) doi:10.1016/j.cub.2009.07.004.

71. Archibald, J. M., Simpson, A. G. B. & Slamovits, C. H. *Handbook of the Protists*. *Handbook of the Protists* (Springer International Publishing, 2017). doi:10.1007/978-3-319-32669-6.

72. Huerta-Cepas, J. *et al.* Fast genome-wide functional annotation through orthology assignment by eggNOG-mapper. *Mol. Biol. Evol.* **34**, 2115–2122 (2017).

73. Cuomo, C. A. *et al.* Microsporidian genome analysis reveals evolutionary strategies for obligate intracellular growth. *Genome Res.* (2012) doi:10.1101/gr.142802.112.

74. Nakjang, S. *et al.* Reduction and expansion inmicrosporidian genome evolution: New insights from comparative genomics. *Genome Biol. Evol.* (2013) doi:10.1093/gbe/evt184.

75. Vivarès, C. P., Gouy, M., Thomarat, F. & Méténier, G. Functional and evolutionary analysis of a eukaryotic parasitic genome. *Current Opinion in Microbiology* (2002) doi:10.1016/S1369-5274(02)00356-9.

76. Corsaro, D. *et al.* Microsporidia-like parasites of amoebae belong to the early fungal lineage Rozellomycota. *Parasitol. Res.* **113**, 1909–1918 (2014).

77. Ho, Y. W. & Barr, D. J. S. Classification of anaerobic gut fungi from herbivores with emphasis on rumen fungi from Malaysia. *Mycologia* (1995) doi:10.2307/3760810.

78. Powell, M. J. Chytridiomycota. in *Handbook of the Protists: Second Edition* (2017).

854 doi:10.1007/978-3-319-28149-0_18.
855 79. Ogata, H. *et al.* KEGG: Kyoto encyclopedia of genes and genomes. *Nucleic Acids Research* (1999)
856 doi:10.1093/nar/27.1.29.
857 80. Gissi, C., Iannelli, F. & Pesole, G. Evolution of the mitochondrial genome of Metazoa as
858 exemplified by comparison of congeneric species. *Heredity* (2008) doi:10.1038/hdy.2008.62.
859 81. Egger, B., Bachmann, L. & Fromm, B. Atp8 is in the ground pattern of flatworm mitochondrial
860 genomes. *BMC Genomics* (2017) doi:10.1186/s12864-017-3807-2.
861 82. Agrawal, Y., Khatri, I., Subramanian, S. & Shenoy, B. D. Genome sequence, comparative analysis,
862 and evolutionary insights into chitinases of entomopathogenic fungus *Hirsutella thompsonii*.
863 *Genome Biol. Evol.* (2015) doi:10.1093/gbe/evv037.
864 83. de Oliveira, E. S. *et al.* Molecular evolution and transcriptional profile of GH3 and GH20 β-n-
865 acetylglucosaminidases in the entomopathogenic fungus *Metarhizium anisopliae*. *Genet. Mol. Biol.*
866 (2018) doi:10.1590/1678-4685-gmb-2017-0363.
867 84. Cavalier-Smith, T. & Chao, E. E. Y. Phylogeny of choanozoa, apusozoa, and other protozoa and
868 early eukaryote megaevolution. *J. Mol. Evol.* (2003) doi:10.1007/s00239-002-2424-z.
869 85. Torruella, G. *et al.* Phylogenomics reveals convergent evolution of lifestyles in close relatives of
870 animals and fungi. *Curr. Biol.* **25**, 2404–2410 (2015).
871 86. Naranjo-Ortiz, M. A. & Gabaldón, T. Fungal evolution: major ecological adaptations and
872 evolutionary transitions. *Biol. Rev.* **94**, 1443–1476 (2019).
873 87. Letcher, P. M. & Powell, M. J. A taxonomic summary and revision of *Rozella* (Cryptomycota). *IMA*
874 *Fungus* **9**, 383–399 (2018).
875 88. Hibbett, D. S. *et al.* A higher-level phylogenetic classification of the Fungi. *Mycol. Res.* (2007)
876 doi:10.1016/j.mycres.2007.03.004.
877 89. Mitchell, D. R. Speculations on the evolution of 9+2 organelles and the role of central pair
878 microtubules. *Biology of the Cell* (2004) doi:10.1016/j.biolcel.2004.07.004.
879 90. Letcher, P. M. *et al.* An ultrastructural study of *Paraphysoderma sedebokerense*
880 (Blastocladiomycota), an epibiotic parasite of microalgae. *Fungal Biol.* **120**, 324–337 (2016).
881 91. Strittmatter, M., Guerra, T., Silva, J. & Gachon, C. M. M. A new flagellated dispersion stage in
882 *Paraphysoderma sedebokerense*, a pathogen of *Haematococcus pluvialis*. *J. Appl. Phycol.* **28**,
883 1553–1558 (2016).
884 92. Sparrow, F. K. Aquatic Phycomycetes. *Univ. Michigan Press* **132**, (1960).
885 93. Powell, M. J. Blastocladiomycota. in *Handbook of the Protists: Second Edition* (2017).
886 doi:10.1007/978-3-319-28149-0_17.
887 94. Aubusson-Fleury, A. *et al.* Centrin diversity and basal body patterning across evolution: New

insights from *Paramecium*. *Biol. Open* **6**, 765–776 (2017).

95. Dupuis-Williams, P. *et al.* Functional role of ε-tubulin in the assembly of the centriolar microtubule scaffold. *J. Cell Biol.* **158**, 1183–1193 (2002).

96. Forget, L., Ustinova, J., Wang, Z., Huss, V. A. R. & Lang, B. F. *Hyaloraphidium curvatum*: A linear mitochondrial genome, tRNA editing, and an evolutionary link to lower fungi. *Mol. Biol. Evol.* (2002) doi:10.1093/oxfordjournals.molbev.a004084.

97. McKerracher, L. J. & Heath, I. B. The structure and cycle of the nucleus-associated organelle in two species of *Basidiobolus*. *Mycologia* (1985) doi:10.2307/3793197.

98. Roberson, R. W. *et al.* The hyphal tip structure of *Basidiobolus* sp.: A zygomycete fungus of uncertain phylogeny. *Fungal Biol.* (2011) doi:10.1016/j.funbio.2011.02.012.

99. McLaughlin, D. J., Healy, R. A., Celio, G. J., Roberson, R. W. & Kumar, T. K. A. Evolution of zygomycetous spindle pole bodies: Evidence from *Coemansia reversa* mitosis. *Am. J. Bot.* (2015) doi:10.3732/ajb.1400477.

100. Fabel, P., Radek, R. & Storch, V. A new spore-forming protist, *Nephridiophaga blaberi* sp. nov., in the Death's head cockroach *Blaberus craniifer*. *Eur. J. Protistol.* (2000) doi:10.1016/S0932-4739(00)80044-9.

101. Radek, R. *et al.* Morphologic and molecular data help adopting the insect-pathogenic nephridiophagids (Nephridiophagidae) among the early diverging fungal lineages, close to the Chytridiomycota. *MycoKeys* (2017) doi:10.3897/mycokeys.25.12446.

102. Strassert, J. F. H. *et al.* Long rDNA amplicon sequencing of insect-infecting nephridiophagids reveals their affiliation to the Chytridiomycota (Fungi) and a potential to switch between hosts. *bioRxiv* (2020) doi:10.1101/2020.10.14.339143.

103. Belas, R., Simon, M. & Silverman, M. Regulation of lateral flagella gene transcription in *Vibrio parahaemolyticus*. *J. Bacteriol.* **167**, 210–218 (1986).

104. Belas, R. Biofilms, flagella, and mechanosensing of surfaces by bacteria. *Trends Microbiol.* **22**, 517–527 (2014).

105. Wang, Q., Suzuki, A., Mariconda, S., Porwollik, S. & Harshey, R. M. Sensing wetness: A new role for the bacterial flagellum. *EMBO J.* **24**, 2034–2042 (2005).

106. Lovett, J. S. Growth and differentiation of the water mold *Blastocladiella emersonii*: cytodifferentiation and the role of ribonucleic acid and protein synthesis. *Bacteriol. Rev.* **39**, 345–404 (1975).

107. Avelar, G. M. *et al.* A Rhodopsin-Guanylyl cyclase gene fusion functions in visual perception in a fungus. *Curr. Biol.* **24**, 1234–1240 (2014).

108. Avelar, G. M. *et al.* A cyclic GMP-dependent K+ channel in the blastocladiomycete fungus

Blastocladiella emersonii. *Eukaryot. Cell* **14**, 958–963 (2015).

109. Richards, T. A. & Gomes, S. L. How to build a microbial eye. *Nature* **523**, 166–167 (2015).

110. Ernst, O. P. *et al.* Microbial and animal rhodopsins: Structures, functions, and molecular mechanisms. *Chemical Reviews* (2014) doi:10.1021/cr4003769.

111. Needham, D. M. *et al.* A distinct lineage of giant viruses brings a rhodopsin photosystem to unicellular marine predators. *Proc. Natl. Acad. Sci. U. S. A.* (2019) doi:10.1073/pnas.1907517116.

112. Wöstemeyer, J., Grünler, A., Schimek, C. & Voigt, K. Genetic regulation of carotenoid biosynthesis in fungi. in *Applied Mycology and Biotechnology* (2005). doi:10.1016/S1874-5334(05)80013-9.

113. Nagy, L. G., Kovács, G. M. & Krizsán, K. Complex multicellularity in fungi: evolutionary convergence, single origin, or both? *Biol. Rev.* **93**, 1778–1794 (2018).

114. Kiss, E. *et al.* Comparative genomics reveals the origin of fungal hyphae and multicellularity. *Nat. Commun.* **10**, (2019).

115. Andrews, S. FastQC: A quality control tool for high throughput sequence data. *Http://Www.Bioinformatics.Babraham.Ac.Uk/Projects/Fastqc/* http://www.bioinformatics.babraham.ac.uk/projects/ (2010) doi:citeulike-article-id:11583827.

116. Bolger, A. M., Lohse, M. & Usadel, B. Trimmomatic: A flexible trimmer for Illumina sequence data. *Bioinformatics* **30**, 2114–2120 (2014).

117. Bankevich, A. *et al.* SPAdes: A new genome assembly algorithm and Its applications to single-cell sequencing. *J. Comput. Biol.* **19**, 455–477 (2012).

118. Laetsch, D. R. & Blaxter, M. L. BlobTools: Interrogation of genome assemblies. *F1000Research* **6**, 1287 (2017).

119. Li, W. & Godzik, A. Cd-hit: A fast program for clustering and comparing large sets of protein or nucleotide sequences. *Bioinformatics* (2006) doi:10.1093/bioinformatics/btl158.

120. Camacho, C. *et al.* BLAST+: Architecture and applications. *BMC Bioinformatics* (2009) doi:10.1186/1471-2105-10-421.

121. Gurevich, A., Saveliev, V., Vyahhi, N. & Tesler, G. QUAST: Quality assessment tool for genome assemblies. *Bioinformatics* **29**, 1072–1075 (2013).

122. Okonechnikov, K., Conesa, A. & García-Alcalde, F. Qualimap 2: Advanced multi-sample quality control for high-throughput sequencing data. *Bioinformatics* **32**, 292–294 (2015).

123. Altschul, S. F., Gish, W., Miller, W., Myers, E. W. & Lipman, D. J. Basic local alignment search tool. *J. Mol. Biol.* **215**, 403–410 (1990).

124. Bernt, M. *et al.* MITOS: Improved de novo metazoan mitochondrial genome annotation. *Mol. Phylogenet. Evol.* (2013) doi:10.1016/j.ympev.2012.08.023.

125. Katoh, K. & Standley, D. M. MAFFT multiple sequence alignment software version 7:

Improvements in performance and usability. *Mol. Biol. Evol.* **30**, 772–780 (2013).

126. Capella-Gutiérrez, S., Silla-Martínez, J. M. & Gabaldón, T. trimAl: A tool for automated alignment trimming in large-scale phylogenetic analyses. *Bioinformatics* **25**, 1972–1973 (2009).

127. Kearse, M. *et al.* Geneious Basic: An integrated and extendable desktop software platform for the organization and analysis of sequence data. *Bioinformatics* **28**, 1647–1649 (2012).

128. Price, M. N., Dehal, P. S. & Arkin, A. P. Fasttree: Computing large minimum evolution trees with profiles instead of a distance matrix. *Mol. Biol. Evol.* (2009) doi:10.1093/molbev/msp077.

129. Lartillot, N., Lepage, T. & Blanquart, S. PhyloBayes 3: A Bayesian software package for phylogenetic reconstruction and molecular dating. *Bioinformatics* (2009) doi:10.1093/bioinformatics/btp368.

130. Nguyen, L. T., Schmidt, H. A., Von Haeseler, A. & Minh, B. Q. IQ-TREE: A fast and effective stochastic algorithm for estimating maximum-likelihood phylogenies. *Mol. Biol. Evol.* **32**, 268–274 (2015).

131. Minh, B. Q., Nguyen, M. A. T. & Von Haeseler, A. Ultrafast approximation for phylogenetic bootstrap. *Mol. Biol. Evol.* (2013) doi:10.1093/molbev/mst024.

132. Anisimova, M., Gil, M., Dufayard, J. F., Dessimoz, C. & Gascuel, O. Survey of branch support methods demonstrates accuracy, power, and robustness of fast likelihood-based approximation schemes. *Syst. Biol.* (2011) doi:10.1093/sysbio/syr041.

133. Rambaut, A. FigTree v1.4.3. *Molecular evolution, phylogenet ics and epidemiology* (2016).

134. Mesquite Project Team. Mesquite: A modular system for evolutionary analysis. *Available from: http:// mesquiteproject.wikispaces.com/home* (2014) doi:10.1017/CBO9781107415324.004.

135. Felsenstein, J. PHYLIP (Phylogenetic Inference Package, version 3.5c). *Dpartement of Genetics, SK, University of Washington, Seattle, WA* (1993) doi:10.2987/10-6090.1.

136. R Development Core Team, R. *R: A Language and Environment for Statistical Computing*. *R Foundation for Statistical Computing* (2011). doi:10.1007/978-3-540-74686-7.

137. Kanehisa, M., Sato, Y. & Morishima, K. BlastKOALA and GhostKOALA: KEGG tools for functional characterization of genome and metagenome sequences. *J. Mol. Biol.* (2016) doi:10.1016/j.jmb.2015.11.006.

138. Carvalho-Santos, Z., Azimzadeh, J., Pereira-Leal, J. B. & Bettencourt-Dias, M. Tracing the origins of centrioles, cilia, and flagella. *Journal of Cell Biology* (2011) doi:10.1083/jcb.201011152.

139. Wickstead, B. & Gull, K. Evolutionary biology of dyneins. in *Dyneins* (2012). doi:10.1016/B978-0-12-382004-4.10002-0.

140. Van Dam, T. J. P. *et al.* Evolution of modular intraflagellar transport from a coatomer-like progenitor. *Proc. Natl. Acad. Sci. U. S. A.* **110**, 6943–6948 (2013).

141. Kubicek, C. P., Starr, T. L. & Glass, N. L. Plant cell wall – degrading enzymes and their secretion in plant-pathogenic fungi. (2014) doi:10.1146/annurev-phyto-102313-045831.

142. Sista Kameshwar, A. K. & Qin, W. Systematic review of publicly available non-Dikarya fungal proteomes for understanding their plant biomass-degrading and bioremediation potentials. *Bioresources and Bioprocessing* (2019) doi:10.1186/s40643-019-0264-6.

143. Csurös, M. Count: Evolutionary analysis of phylogenetic profiles with parsimony and likelihood. *Bioinformatics* **26**, 1910–1912 (2010).

1000 **Table 1.** Comparative statistics of sanchytrid genomes before and after decontamination with
1001 related zoosporic lineages.

	Amoeboradix gromovi		*Sanchytrium tribonematis*		*Allomyces macrogynus*	*Catenaria anguillulae*	*R. globosum*	*S. punctatus*	*A. robustus*
	Before	After	Before	After					
Genome size (Mb)	48.7	10.5	37.1	11.2	52.62	41.34	57.02	24.1	71.69
GC%	51.06	36.27	42.9	34.64	61.6	56	44.9	47.6	16.3
Number of contigs	8,420	1,167	8,015	1,960	8,973	509	437	329	1,035
N50	27,236	13,376	17,350	11,874	35,497	217,825	292,246	155,888	141,798
Predicted proteins	87,868	7,220	50,780	9,368	19,447	12,763	16,987	9,422	12,083

1002

1003

Fig. 1. **Phylogenomic analysis of Holomycota. a**, Bayesian inference (BI) phylogenomic tree based on 264 conserved proteins. The tree was reconstructed using 69 species and 91,768 amino acid positions with the CAT-Poisson model and the LG+R9+PMSF model for maximum likelihood (ML). Branches with support values higher or equal to 0.99 BI posterior probability and 99% ML bootstrap are indicated by black dots. **b**, Evolution of IQ-TREE ML bootstrap support for Chytridiomycota sister of all other fungi (C+F), Blastocladiomycota + Sanchytriomycota sister of all other fungi (B+F), *Olpidium* independent lineage sister to non-flagellated fungi (O+ZMD), *Olpidium* within Zoopagomycota (O+Z), Sanchytriomycota within Blastocladiomycota (S+B), and the monophyly of Dikarya (Dikarya) as a function of the proportion of fast-evolving sites removed from two datasets (GBE69 without long-branching Microsporidia, and GBE84 with long-branching Microsporidia). The canonical Fungi clade is indicated next to the node. Holomycota are highlighted in violet, sanchytrids in pink and outgroup taxa in other colors. All phylogenomic trees can be seen in Supplementary Figs. 2a-e.

Fig. 2. **Distribution patterns of primary metabolism genes in Holomycota. a**, Binary heat-map and **b**, principal coordinate analysis (PCoA) species clustering based on the presence/absence of 1158 orthologous genes belonging to 8 primary metabolism Gene Ontology categories across 43 eukaryotic genomes and transcriptomes. Species are color- and shaped-coded according to their taxonomic affiliation. COG presence is depicted in blue and absence is depicted in white.

Fig. 3. **Comparison of flagellar protein distribution and structure in sanchytrids and other Holomycota. a**, Presence/absence heatmap of 61 flagellum-specific proteins in 48 eukaryotic flagellated (purple) and non-flagellated (pink) lineages. The right column lists microtubular genes and flagellum-specific genes. **b**, Illustration depicting the main structural elements present in a typical eukaryotic flagellum (left) and a reduced sanchytrid flagellum (right). Gene presence is depicted in blue and absence is depicted in white. **c**, Representation of the evolutionary relationships of holomycotan lineages and their patterns of presence/absence of key molecular components of the flagellar apparatus. Red crosses on branches indicate independent flagellum losses.

Fig. 4. Hyphae-related genes across Holomycota. a, Cladogram of Holomycota depicting the phylogenetic relationships according to the GBE69 phylogenomic reconstruction. Bubble size on the nodes and tips represents the total number of reconstructed ancestral and extant hyphal multicellularity-related proteins. CBOZ (Chytridiomycota, Blastocladiomycota, Olpidiomycota and Zoopagomycota) and NRA (Nucleariids, Rozellida-Microsporidia and Aphelida) nodes are indicated with letters within the corresponding bubbles. Unicellular lineages are highlighted in colors according to their taxonomic affiliation (bottom to top: Amoebozoa, Apusomonadida, nucleariids, Rozellida-Microsporidia, Aphelida, Chytridiomycota, Sanchytriomycota-Blastocladiomycota, Olpidiomycota and Zoopagomycota). **b**, Presence/absence heatmap of 619 hyphal morphogenesis proteins in 69 unicellular (color-highlighted) and multicellular (not highlighted) eukaryotic proteomes. Gene presence is depicted in blue and absence in white. **c**, Heatmap clustered by similarity showing the correlation between unicellular (color-highlighted) and multicellular (not highlighted) taxa according to the presence/absence of hyphal morphogenesis gene proteins.

a

Acanthamoeba castellanii
Dictyostelium discoideum
Thecamonas trahens
Monosiga brevicollis
Salpingoeca rosetta
Nuclearia thermophila
Parvularia atlantis
Fonticula alba
1/98
Rozella allomycis
Paramicrosporidium saccamoebae
Mitosporidium daphniae
Paraphelidium tribonemae
Hyaloraphidium curvatum
Gonapodya prolifera
Piromyces sp.
Anaeromyces robustus
Neocallimastix californiae
Pecoramyces ruminatium
Synchytrium microbalum
Synchytrium taraxaci
Chytridium lagenaria
Cladochytrium polystomum
Obelidium mucronatum
Rhizoclosmatium globosum
1/70
Caulochytrium protostelioides
Batrachochytrium dendrobatidis
Homolaphlyctis polyrhiza
Spizellomyces punctatus
Rhizophlyctis rosea
Blyttiomyces helicus
Fungi
Sanchytrium tribonematis
Amoeboradix gromovi
Paraphysoderma sedebokerensis
Coelomomyces lativittatus
Allomyces macrogynus
Blastocladiella emersonii
Catenaria anguillulae
Blastocladiella britannica
Olpidium bornovanus
1/79
Basidiobolus meristosporus
Basidiobolus heterosporus
Piptocephalis cylindrospora
Conidiobolus coronatus
Entomophthora muscae
Massospora cicadina
0.51/---
Linderina pennispora
Coemansia reversa
Capniomyces stellatus
0.51/---
Smittium culicis
Mortierella verticillata
Mortierella alpina
Umbelopsis isabellina
Lichtheimia hyalospora
1/96
Phycomyces blakesleeanus
Rhizopus oryzae
Mucor circinelloides
Cokeromyces recurvatus
1/98
Rhizophagus irregularis
Glomus cerebriforme
Puccinia graminis
Ustilago maydis
Cryptococcus neoformans
1/---
Postia placenta
Laccaria bicolor
Saitoella complicata
Schizosaccharomyces pombe
Sclerotinia sclerotiorum
Yarrowia lipolytica
0.2
1/---
Saccharomyces cerevisiae

Amoebozoa
Apusomonadida
Holozoa
nucleariids
Microsporidia + Rozellida
Aphelida
Chytridiomycota
Sanchytriomycota
Blastocladiomycota
Olpidiomycota
Zoopagomycota
"Zygomycota"
Mucoromycota
Glomeromycota
Basidiomycota
Ascomycota
Dikarya

b

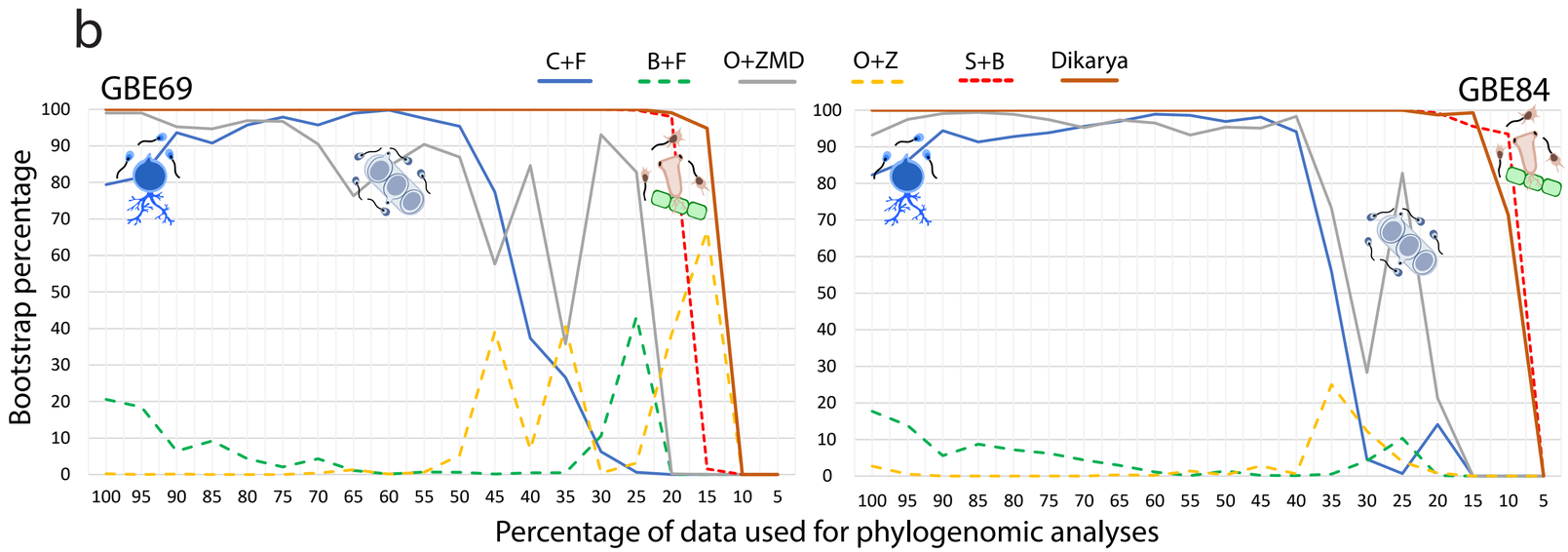

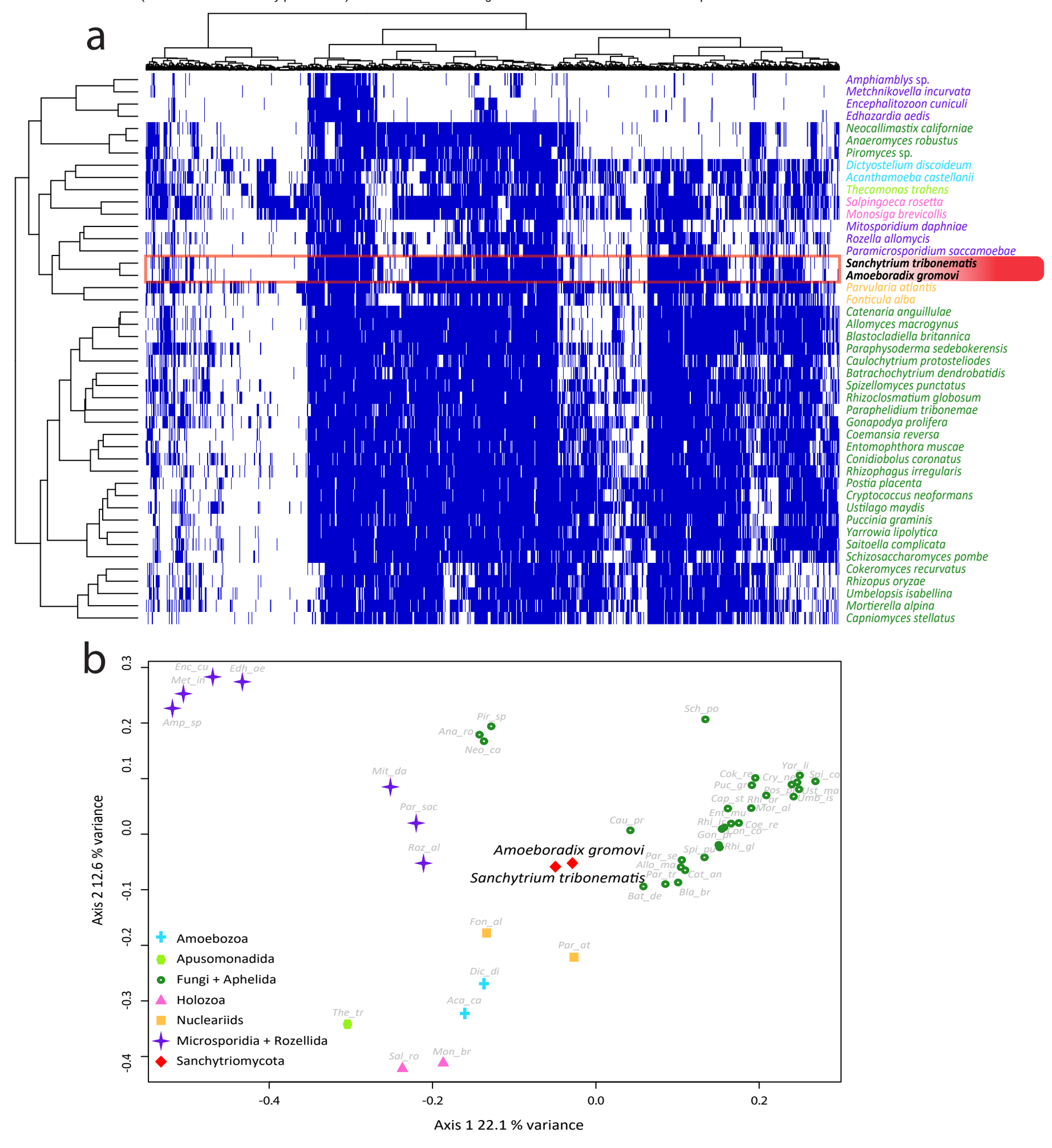
a
Amphiamblys sp.
Metchnikovella incurvata
Encephalitozoon cuniculi
Edhazardia aedis
Neocallimastix californiae
Anaeromyces robustus
Piromyces sp.
Dictyostelium discoideum
Acanthamoeba castellanii
Thecamonas trahens
Salpingoeca rosetta
Monosiga brevicollis
Mitosporidium daphniae
Rozella allomycis
Paramicrosporidium saccamoebae
Sanchytrium tribonematis
Amoeboradix gromovi
Parvularia atlantis
Fonticula alba
Catenaria anguillulae
Allomyces macrogynus
Blastocladiella britannica
Paraphysoderma sedebokerensis
Caulochytrium protosteliodes
Batrachochytrium dendrobatidis
Spizellomyces punctatus
Rhizoclosmatium globosum
Paraphelidium tribonemae
Gonapodya prolifera
Coemansia reversa
Entomophthora muscae
Conidiobolus coronatus
Rhizophagus irregularis
Postia placenta
Cryptococcus neoformans
Ustilago maydis
Puccinia graminis
Yarrowia lipolytica
Saitoella complicata
Schizosaccharomyces pombe
Cokeromyces recurvatus
Rhizopus oryzae
Umbelopsis isabellina
Mortierella alpina
Capniomyces stellatus
b
Axis 2 12.6 % variance
Axis 1 22.1 % variance
0.3
0.2
0.1
0.0
-0.1
-0.2
-0.3
-0.4
-0.4
-0.2
0.0
0.2
Enc_cu
Edh_ae
Met_in
Amp_sp
Pir_sp
Ana_ro
Neo_ca
Sch_po
Mit_da
Par_sac
Roz_al
Cau_pr
Amoeboradix gromovi
Sanchytrium tribonematis
Par_se
Allo_ma
Par_tr
Cat_an
Bat_de
Bla_br
Spi_pu
Rhi_gl
Fon_al
Par_at
Dic_di
Aca_ca
The_tr
Sal_ro
Mon_br
Amoebozoa
Apusomonadida
Fungi + Aphelida
Holozoa
Nucleariids
Microsporidia + Rozellida
Sanchytriomycota

a

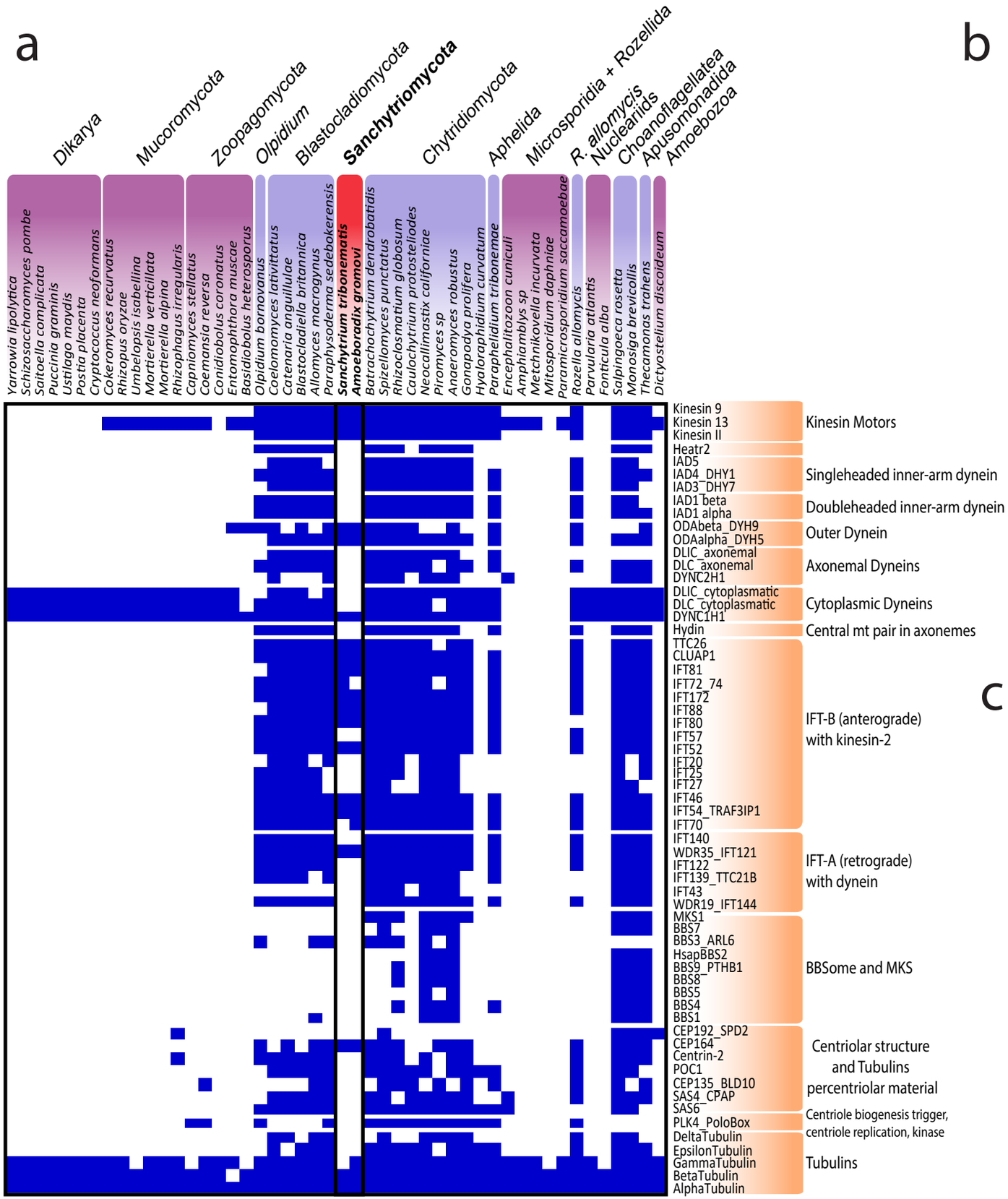
Dikarya
Mucoromycota
Zoopagomycota
Olpidium
Blastocladiomycota
Sanchytriomycota
Chytridiomycota
Aphelida
Microsporidia + Rozellida
R. allomycis
Nucleariids
Choanoflagellatea
Apusomonadida
Amoebozoa
Yarrowia lipolytica
Schizosaccharomyces pombe
Saitoella complicata
Puccinia graminis
Ustilago maydis
Postia placenta
Cryptococcus neoformans
Cokeromyces recurvatus
Rhizopus oryzae
Umbelopsis isabellina
Mortierella verticillata
Mortierella alpina
Rhizophagus irregularis
Capniomyces stellatus
Coemansia reversa
Conidiobolus coronatus
Entomophthora muscae
Basidiobolus heterosporus
Olpidium bornovanus
Coelomomyces lativittatus
Catenaria anguillulae
Blastocladiella britannica
Allomyces macrogynus
Paraphysoderma sedebokerensis
Sanchytrium tribonematis
Amoeboradix gromovi
Batrachochytrium dendrobatidis
Spizellomyces punctatus
Rhizoclosmatium globosum
Caulochytrium protostelioides
Neocallimastix californiae
Piromyces sp
Anaeromyces robustus
Gonapodya prolifera
Hyaloraphidium curvatum
Paraphelidium tribonemae
Encephalitozoon cuniculi
Amphiamblys sp
Metchnikovella incurvata
Mitosporidium daphniae
Paramicrosporidium saccamoebae
Rozella allomycis
Parvularia atlantis
Fonticula alba
Salpingoeca rosetta
Monosiga brevicollis
Thecamonas trahens
Dictyostelium discoideum
Kinesin 9
Kinesin 13
Kinesin II
Kinesin Motors
Heatr2
IAD5
IAD4_DHY1
IAD3_DHY7
Singleheaded inner-arm dynein
IAD1_beta
IAD1 alpha
Doubleheaded inner-arm dynein
ODAbeta_DYH9
ODAalpha_DYH5
Outer Dynein
DLIC_axonemal
DLC_axonemal
DYNC2H1
Axonemal Dyneins
DLIC_cytoplasmatic
DLC_cytoplasmatic
DYNC1H1
Cytoplasmic Dyneins
Hydin
Central mt pair in axonemes
TTC26
CLUAP1
IFT81
IFT72_74
IFT172
IFT88
IFT80
IFT57
IFT52
IFT20
IFT25
IFT27
IFT46
IFT54_TRAF3IP1
IFT70
IFT-B (anterograde) with kinesin-2
IFT140
WDR35_IFT121
IFT122
IFT139_TTC21B
IFT43
WDR19_IFT144
IFT-A (retrograde) with dynein
MKS1
BBS7
BBS3_ARL6
HsapBBS2
BBS9_PTHB1
BBS8
BBS5
BBS4
BBS1
BBSome and MKS
CEP192_SPD2
CEP164
Centrin-2
POC1
CEP135_BLD10
SAS4_CPAP
SAS6
Centriolar structure and Tubulins percentriolar material
PLK4_PoloBox
Centriole biogenesis trigger, centriole replication, kinase
DeltaTubulin
EpsilonTubulin
GammaTubulin
BetaTubulin
AlphaTubulin
Tubulins

b

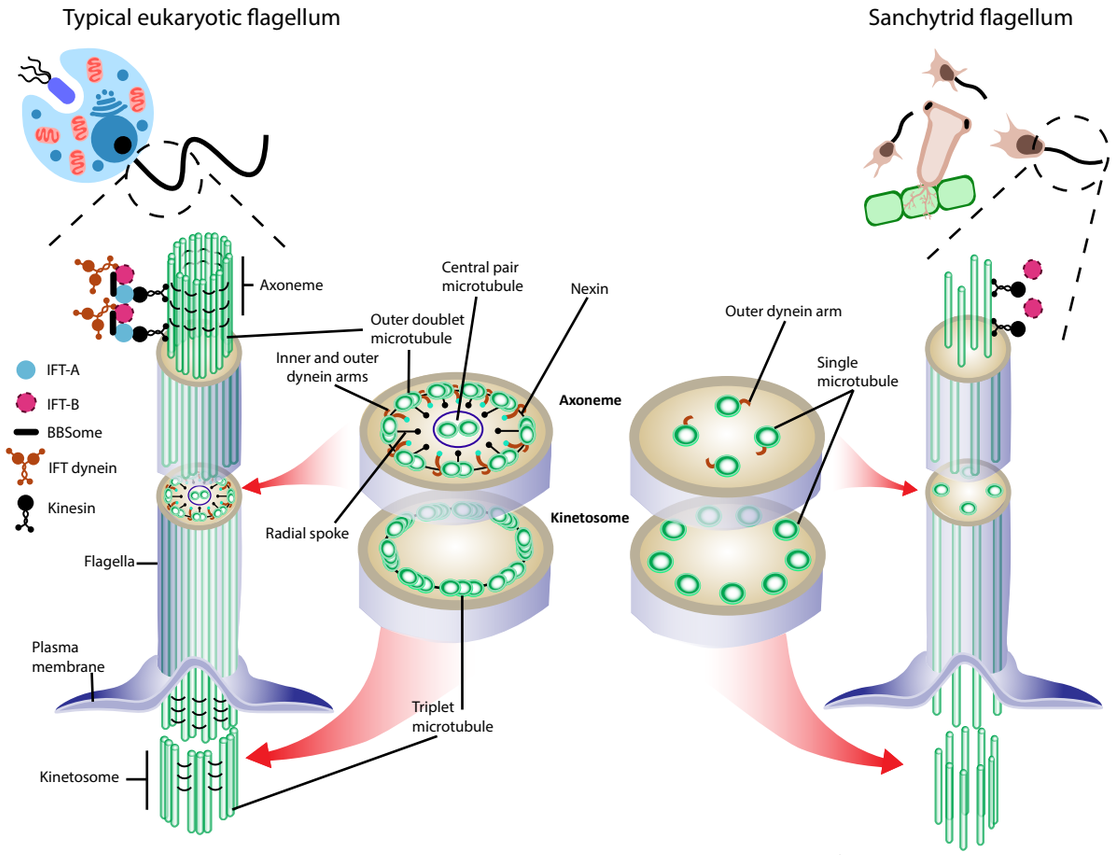
Typical eukaryotic flagellum
Sanchytrid flagellum
Axoneme
Central pair microtubule
Nexin
Outer doublet microtubule
Inner and outer dynein arms
Radial spoke
Flagella
Plasma membrane
Kinetosome
Triplet microtubule
IFT-A
IFT-B
BBSome
IFT dynein
Kinesin
Outer dynein arm
Single microtubule

c

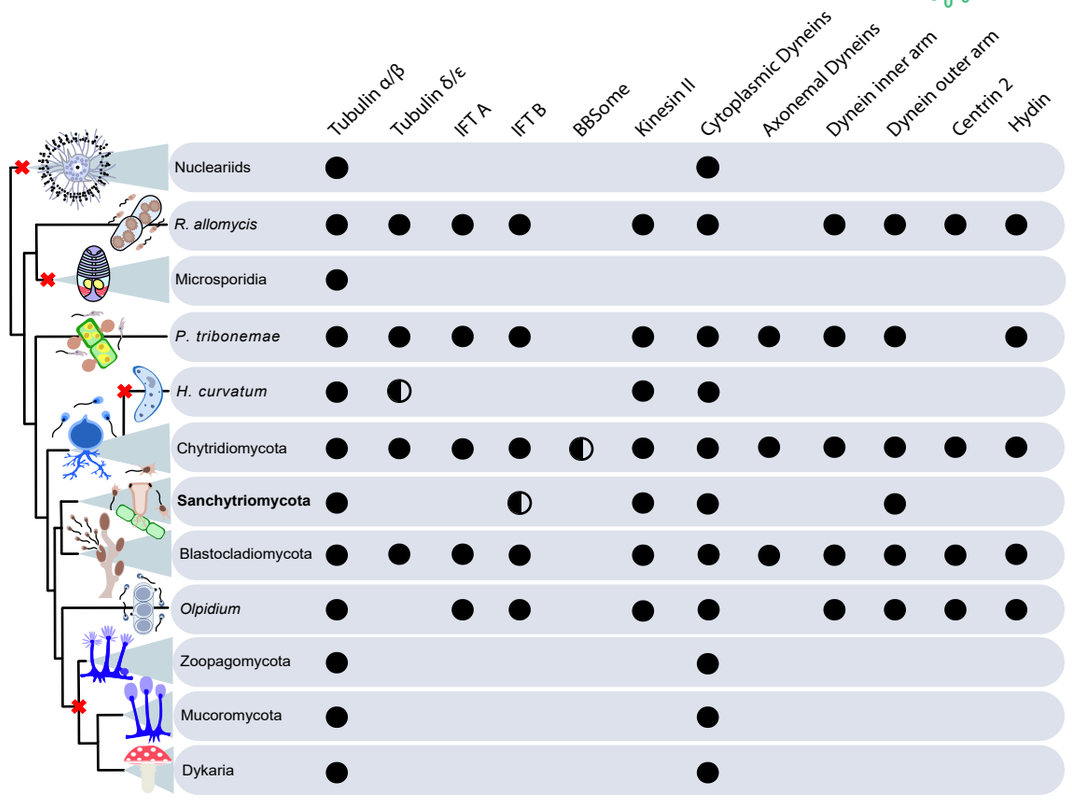
Tubulin α/β
Tubulin δ/ε
IFT A
IFT B
BBSome
Kinesin II
Cytoplasmic Dyneins
Axonemal Dyneins
Dynein inner arm
Dynein outer arm
Centrin 2
Hydin
Nucleariids
R. allomycis
Microsporidia
P. tribonemae
H. curvatum
Chytridiomycota
Sanchytriomycota
Blastocladiomycota
Olpidium
Zoopagomycota
Mucoromycota
Dykaria

a

Number of hyphal multicellularity-related genes (Total gene Nº = 619)

≤ 300
301 - 350
351 - 400
401 - 450
451 - 500
≥501

Z
O
B
C
A
R
N
H

Laccaria bicolor
Postia placenta
Cryptococcus neoformans
Ustilago maydis
Puccinia graminis
Saccharomyces cerevisiae
Yarrowia lipolytica
Sclerotinia sclerotiorum
Schizosaccharomyces pombe
Saitoella complicata
Glomus cerebriforme
Rhizophagus irregularis
Cokeromyces recurvatus
Mucor circinelloides
Rhizopus oryzae
Phycomyces blakesleeanus
Lichtheimia hyalospora
Umbelopsis isabellina
Mortierella alpina
Mortierella verticillata
Capniomyces stellatus
Smittium culicis
Coemansia reversa
Linderina pennispora
Entomophthora muscae
Massospora cicadina
Conidiobolus coronatus
Piptocephalis cylindrospora
Basidiobolus heterosporus
Basidiobolus meristosporus
Olpidium bornovanus
Blastocladiella britannica
Catenaria anguillulae
Blastocladiella emersonii
Allomyces macrogynus
Coelomomyces lativittatus
Paraphysoderma sedebokerensis
Amoeboradix gromovi
Sanchytrium tribonematis
Blyttiomyces helicus
Rhizophlyctis rosea
Spizellomyces punctatus
Batrachochytrium dendrobatidis
Homolaphlyctis polyrhiza
Caulochytrium protosteliodes
Obelidium mucronatum
Rhizoclosmatium globosum
Cladochytrium polystomum
Chytridium lagenaria
Synchytrium microbalum
Synchytrium taraxaci
Neocallimastix californiae
Pecoramyces ruminantium
Anaeromyces robustus
Piromyces sp.
Gonapodya prolifera
Hyaloraphidium curvatum
Paraphelidium tribonemae
Mitosporidium daphniae
Paramicrosporidium saccamoebae
Rozella allomycis
Fonticula alba
Parvularia atlantis
Nuclearia thermophila
Monosiga brevicollis
Salpingoeca rosetta
Thecamonas trahens
Dictyostelium discoideum
Acanthamoeba castellanii

b

Blyttiomyces helicus
Homolaphlyctis polyrhiza
Pecoramyces ruminatium
Rhizophlyctis rosea
Olpidium bornovanus
Synchytrium taraxaci
Piptocephalis cylindrospora
Blastocladiella emersonii
Mitosporidium daphniae
Parvularia atlantis
Fonticula alba
Nuclearia thermophila
Blastocladiella britannica
Chytridium lagenaria
Synchytrium microbalum
Cladochytrium polystomum
Coelomomyces lativittatus
Paraphelidium tribonemae
Paraphysoderma sedebokerensis
Rhizoclosmatium globosum
Obelidium mucronatum
Hyaloraphidium curvatum
Caulochytrium protosteliodes
Glomus cerebriforme
Rhizophagus irregularis
Neocallimastix californiae
Anaeromyces robustus
Piromyces sp.
Sanchytrium tribonematis
Amoeboradix gromovi
Paramicrosporidium sacamoebae
Sclerotinia sclerotiorum
Postia placenta
Yarrowia lipolytica
Saitoella complicata
Linderina pennispora
Entomophthora muscae
Lichtheimia hyalospora
Mortierella verticillata
Basidiobolus meristosporus
Smittium culicis
Capniomyces stellatus
Massospora cicadina
Basidiobolus heterosporus
Umbelopsis isabellina
Mortierella alpina
Cokeromyces recurvatus
Thecamonas trahens
Dictyostelium discoideum
Acanthamoeba castellanii
Saccharomyces cerevisiae
Phycomyces blakesleeanus
Coemansia reversa
Conidiobolus coronatus
Mucor circinelloides
Rhizopus oryzae
Schizosaccharomyces pombe
Laccaria bicolor
Cryptococcus neoformans
Ustilago maydis
Puccinia graminis
Batrachochytrium dendrobatidis
Gonapodya prolifera
Spizellomyces punctatus
Rozella allomycis
Catenaria anguillulae
Allomyces macrogynus
Salpingoeca rosetta
Monosiga brevicollis

C